Phase-resolved time-domain nonlinear optical signals

Sarah M. Gallagher Faeder,* and David M. Jonas[†]

Department of Chemistry and Biochemistry, University of Colorado, Boulder, Colorado 80309-0215

A systematic theoretical and computational investigation of the microscopic factors which determine the phase of the signal field in time-resolved quasidegenerate three-pulse scattering experiments is presented. The third-order phase-matched response is obtained by density-matrix perturbation theory using a Green-function formalism for a system composed of two well-separated sets of closely spaced energy levels. Equations for calculating the electric field of four-wave-mixing signals generated by path-length delayed pulses are given. It is found that the phase of the signal field is determined by the excitation pulse phases, the dynamics of the nonlinear polarization decay, the product of four transition dipole matrix elements, and by a pulse-delay-dependent phase modulation at the frequency of the first dipole oscillation in the four-wave-mixing process. Analytic results for a two-level Bloch model show the phase shift from rapid nonlinear polarization decay. The product of dipole matrix elements is real and positive for three-level processes (bleached ground-state absorption and excited-state emission), but can be real and negative for some four-level Raman processes. The pulse-delay-dependent phase modulation treated here is closely related to the interferometric pulse-delay-dependent amplitude modulation observed in some collinear experiments, and plays a role in producing photon echos in inhomogeneously broadened samples. Numerical calculations of phase-resolved electric fields for finite duration pulses using a Brownian oscillator model appropriate for condensed-phase dynamics are presented. The ability of pulse-delay-dependent phase modulation to encode the frequency of the initially excited dipole onto the phase of the signal field can be exploited to examine energy-level connectivity, reveal correlations hidden under the inhomogeneous lineshape, and probe relaxation pathways in multilevel systems.

PACS number(s): 42.65.Dr, 42.50.Md, 78.47.+p

I. INTRODUCTION

Since the pioneering work of Ref. [1], photon echos and related four-wave-mixing experiments have been used to probe molecular dynamics which are hidden by macroscopic inhomogeneous broadening [2–10]. Relative phases between different contributions to the signal were experimentally significant because they produced detectable modulations of the total signal energy as a function of pulse delay [6,8–17], but the overall phase of the signal could not be measured, and was usually ignored in discussions of fully noncollinear experiments. In partly collinear experiments, where the signal phase is relevant to the detected intensity [2], the available bandwidth allowed phase shifts and time delays to be treated interchangeably. An experimental distinction becomes possible for pulses consisting of a few optical cycles [18].

In the past few years, there has been a dramatic improvement in methods for characterizing femtosecond optical pulses [19–26], and a corresponding increase in the level of characterization of nonlinear optical signals [27–36]. A pulse has usually been considered fully characterized when instantaneous amplitude and frequency are both known [19,23,26]. This information can be obtained from frequency-resolved optical gating [19,20,22,23,25,26], and

displayed in a spectrogram [31,35,37]. Recent work suggested a significant role for constant terms in the pulse phase in extreme nonlinear optics [18]. To date, no measurement of the constant term in the phase of a pulse has been demonstrated. As a method of signal characterization, the heterodyne sensitivity and multiplex advantage of spectral interferometry have attracted much attention [21,24,27,29,31–34]. Recently, it was demonstrated that spectral interferometry can independently measure both time delays and constant spectral phase shifts between pulses [38]. It is now possible to measure the electric field of femtosecond four-wave-mixing signals at the point they exit a sample, including constant phase shifts of the signal field relative to the excitation pulses [35]. Thus, unlike frequency-resolved optical gating, spectral interferometry is capable of *completely* characterizing a perturbative nonlinear optical response. The interpretation of such experiments has necessitated a systematic treatment of the phase shift of nonlinear optical signals relative to the excitation pulses presented here.

The pulse sequence for a three-pulse scattering experiment is shown in Fig. 1. In these experiments, all three excitation pulses are noncollinear, and a phase-matched signal is radiated into a fourth background-free direction. Most of the factors contributing to the fully noncollinear signal phase also affect the energy of partly collinear signals. Aside from the effect of excitation pulse phase [35,39–43] and resonance detuning [29,36,40,44], the influence of pulse delay [12] and a product of four transition dipole moments [45] on the signal phase have been briefly mentioned. Two other phase factors were mentioned only recently. The first stems from the form of the delayed pulses. Selecting slices from a single, continuous carrier wave [46], generates ``carrier-

————

*Present address: Department of Physics of Complex Systems, Weizmann Institute of Science, 76100 Rehovot, Israel.

[†]Corresponding author. Mailing address: Department of Chemistry and Biochemistry, CB 215, University of Colorado at Boulder, Boulder, CO 80309-0215. FAX:(303)492-5894. Email address: David.Jonas@Colorado.edu
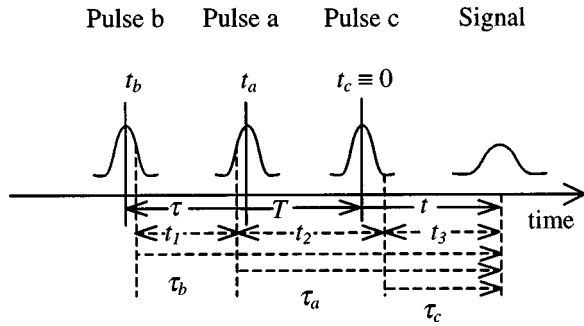
FIG. 1. Illustration of time variables for three pulse-scattering sequence b, a, and c. The times t_a, t_b, and t_c label experimentally controlled arrival times of the pulse centers at the sample. t is the running time after the arrival of the last pulse (c) at $t_c = 0$. For a three-pulse echo, the arrival times t_a and t_b are both negative, but pulses a and b can arrive in either order. The standard three-pulse scattering delay variables $\tau \equiv t_b - t_a$, and $T = t_c - \max(t_a, t_b)$ are also shown. At a given time t, the polarization depends on the values of the excitation fields at all times in the past. Positive times τ_a, τ_b, and τ_c label the interval between t and the perturbation theoretic interactions with pulses a, b, and c, respectively. The positive time intervals between perturbation theoretic interactions are always numbered consecutively as t_1, t_2, and t_3.

wave-delayed'' pulses of the form $E(t) = e(t - t_d)\cos(\omega_0 t)$, where $e(t)$ is the pulse envelope, t_d is the delay, and ω_0 is the continuous carrier wave frequency. The pulses generated by lengthening one arm of an interferometer are of the ''envelope-delayed'' form, $E(t) = e(t - t_d)\cos[\omega_0(t - t_d)]$, which differs from the carrier wave form by a delay-dependent temporal phase shift $-\omega_0 t_d$. We have briefly indicated how envelope-delayed pulses can encode the dipole oscillation frequency between the first two pulses onto the signal phase [38], and the treatment is extended to temporally overlapping pulses here. A second new phase shift arises from radiation by a nonlinear polarization that decays within a few optical cycles. Related distortions of the signal spectrum were discussed in two recent treatments of frequency-resolved optical gating [25,26]. In the time domain, polarization radiation can produce constant phase shifts, frequency chirps, and temporal modulations of the signal field which are not present in the source polarization.

Envelope pulse delays have been used to treat second-order nonlinear processes. In Weiner's discussion of noncollinear second-order autocorrelation as a technique for measuring pulse duration [47], Eq. (4) predicts a pulse-delay-dependent phase modulation of the second-harmonic field at the fundamental frequency. This same phase modulation is also implicitly present in the frequency-domain expression [Eq. (1)] used by Lepetit, Cheriaux, and Joffre [30] to simulate their absolute value map of the two-dimensional nonlinear response of a potassium di-hydrogen phosphate (KDP) crystal, but the phase modulation explicitly appeared at the difference frequency because of the way they defined the delay and time origin. A one-dimensional Fourier transform sum-frequency experiment based on somewhat different principles was recently reported [48].

Equations for calculating the nonlinear polarization in noncollinear (third-order) four-wave-mixing experiments

have usually used carrier wave delays [3,41] or an equivalent rotating frame description [49]. For four-wave-mixing signals generated by two noncollinear pulses, carrier wave delays are adequate to calculate time-integrated signals [41], the temporal envelope of the signal intensity [50,51], the signal spectrogram [37], and the instantaneous time-frequency profile [28,34], even if delays are generated by an interferometer. Systematically undersampled experiments with phase-locked collinear pulses [32,42,43] can be exactly calculated with carrier wave delays by incorporating a small phase-shift-dependent delay $t_d = \phi/\omega_L$ [38]. Recent experiments in which two collinear pulses are delayed by an interferometer in subwavelength steps require envelope delayed pulses to calculate the interferometric amplitude modulation of the signal [52,53], as do noncollinear experiments in which constant phase shifts of the signal relative to the excitation pulses are measured [35,36].

We use a response function formalism based on density-matrix perturbation theory to obtain general expressions for the third-order nonlinear polarization (within the rotating-wave approximation) for pulses delayed by an optical path difference. The electric field of the signal is calculated from the nonlinear polarization using the infinite plane wave and slowly evolving wave approximation [49,54]. On a femto-second time scale, molecular electronic relaxation and dephasing are limited by nuclear motion, in accord with the Franck-Condon principle. The Brownian oscillator model [41] has been widely used to model femtosecond four-wave-mixing experiments, because it allows the nuclei to respond to a change in molecular electronic state and change the electronic frequency as they move. In this paper, response functions based on a Brownian oscillator model are used to calculate the phase-resolved electric fields of femtosecond four-wave-mixing signals. In its simplest form, the Brownian oscillator model treats a quantum-mechanical transition between two electronic states with classical nuclear motions modeled by damped harmonic oscillators subject to random fluctuating forces. The frequency of each oscillator is the same on both the ground and excited electronic states. Each nuclear motion in the system is described by one harmonic frequency, a relative displacement of the ground and excited state potential minima, and a coupling to the bath (i.e., a frictional damping proportional to the mode velocity). The fluctuation-dissipation theorem then dictates the random force required to maintain vibrational thermal equilibrium on each electronic state.

The numerical results show how the amplitude and phase of the signal field are affected by pulse delay, illustrate the effects of finite pulse duration and temporally overlapping pulses, and connect signal phase modulation in noncollinear experiments to amplitude modulation in collinear experiments. When broadband excitation pulses are used, the equations given here show that phase modulation of the signal field with pulse delay can be used to correlate initial and final dipole oscillation frequencies. Such a correlation establishes that the two transitions occur in the same molecule, or that the initial excitation has been transferred to the final emitter by some relaxation pathway. As recently demonstrated by Hybl *et al.* [36], correlations under the inhomogeneous line

shape can be revealed by successive Fourier transformation of four-wave-mixing signal fields with respect to time and pulse delay if the real and imaginary parts of the two-dimensional (2D) spectrum are separated. The treatment of phase-resolved four-wave-mixing fields given here establishes a theoretical foundation for these experiments. The calculation of two-dimensional spectra which separate absorptive and dispersive terms in the nonlinear susceptibility into real and imaginary parts of the 2D spectra presents special problems discussed in a separate paper [55].

II. THEORY

Third-order nonlinear optical signals result from radiation by an electric polarization that is proportional to the third power of the excitation field. This third-order polarization is formally induced by three perturbation theoretic interactions with optical electric fields. If the total polarization can be expanded in a Volterra functional power series [56], the third-order polarization can be written as a triple convolution of the third-order nonlinear response function with three excitation fields [41]. The time-domain electric field $E(t)$ is a real-valued function which can be written as

$$E(t) = e(t)\cos[\phi(t)] \tag{1}$$

where $e(t)$ is the pulse envelope, and $\phi(t)$ is the temporal phase. In practice, the envelope is defined by $e(t) \equiv |(1/\pi)\int_0^\infty \int_{-\infty}^\infty E(t')\exp(i\omega t')dt' \exp(-i\omega t)d\omega|$, and the temporal phase as the negative argument of the complex expression in the absolute value. The time-delayed field produced by an interferometer path-length difference is given by substituting $(t-t_d)$ in place of t everywhere on the right-hand side in Eq. (1). A phase shift is defined as the addition of $\phi_0 \text{sgn}(\omega)$ to the spectral phase, and is equivalent (within the rotating-wave approximation) [38] to subtraction of ϕ_0 from $\phi(t)$. For a causal third-order nonlinear response in a homogeneous and isotropic medium, the nonlinear polarization in four-wave mixing is given by [57]

$$P^{(3)}(t) = \int_0^\infty \int_0^\infty \int_0^\infty \chi^{(3)}(\tau_a, \tau_b, \tau_c) E_a(t-\tau_a) E_b(t-\tau_b)$$

$$\times E_c(t-\tau_c) d\tau_a d\tau_b d\tau_c. \tag{2}$$

At each point in the sample, Eq. (2) relates the nonlinear polarization $P^{(3)}$ at time t to the values of three applied fields at all times in the past. The three field-matter interactions at $t-\tau_a$, $t-\tau_b$, and $t-\tau_c$ can occur in any order. The complete third-order response function $\chi^{(3)}(\tau_a, \tau_b, \tau_c)$ is equal to the polarization created by three δ-function excitation pulses at the times τ_a, τ_b, and τ_c before the present (t).

$\chi^{(3)}(\tau_a, \tau_b, \tau_c)$ can be calculated by third-order perturbation theory. Density-matrix perturbation theory is convenient because each term in the perturbation series has a definite wave vector, so that only terms which contribute to a macroscopically near-phase-matched polarization for the detected signal direction need be retained [41,49]. The resulting phase-matched response $S^{(3)}(\mathbf{k}_s, \tau_a, \tau_b, \tau_c)$ is the directional Fourier component of $P^{(3)}(\mathbf{r},t)$ with wave vector $\mathbf{k}_s$, created by δ-function pulses with wave vectors $\mathbf{k}_\alpha$ hitting
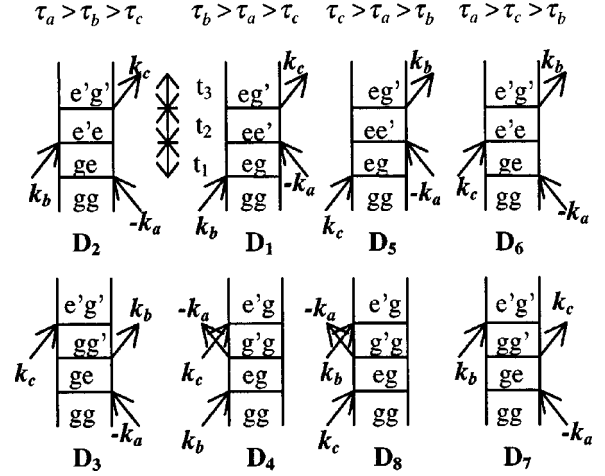
FIG. 2. The eight double-sided Feynman diagrams which survive the rotating-wave approximation for four-wave mixing signals with phase-matching direction $-\mathbf{k}_a+\mathbf{k}_b+\mathbf{k}_c$ in a two-electronic-state system. The arrows represent the three perturbation-theoretic field-matter interactions, one with each applied field. The three fields are distinguished by their wave vectors $-\mathbf{k}_a$, $\mathbf{k}_b$, and $\mathbf{k}_c$. Time increases along the vertical direction. t_1 is the time interval between the first and second interactions, t_2 the time interval between the second and third interactions, and t_3 the time interval between the third interaction and coherent radiation. The two letters in the center of each diagram indicate the density-matrix element probed during each time interval. e and e' designate excited electronic state sublevels, and g and g' designate ground-electronic-state sublevels.

$\mathbf{r}=0$ at times τ_α before the present $(\alpha=a,b,c)$. $S^{(3)}(\mathbf{k}_s, \tau_a, \tau_b, \tau_c)$, is real and depends on both the detected signal wave vector $\mathbf{k}_s$ and the phase-matching geometry. The permutation symmetry of some tensor components of $\chi^{(3)}$ is lowered in $S^{(3)}$ (e.g., $\chi^{(3)}_{xxxx}$ is symmetric with respect to all permutations of τ_α, while fully noncollinear $S^{(3)}_{xxxx}$ has only the intrinsic permutation symmetry in which times τ_α and wave vectors $\mathbf{k}_\alpha$ are both interchanged). For resonant absorption, the rotating-wave approximation is surprisingly accurate for smooth pulse envelopes as short as a single optical cycle [58]. For fully resonant four-wave-mixing signals, one can use the rotating-wave approximation to break the real, amplitude modulated fields and phase-matched response function into complex, phase-modulated parts, and retain only those terms in Eq. (2) for which all of the phase modulations approximately cancel. These complex fields and phase-matched response functions will be denoted $\hat{E}$ and $\hat{S}^{(3)}$.

The model considered here consists of two well-separated sets of closely spaced energy levels approximating the sublevels of two electronic states. The lower levels are denoted g or g' and the upper levels are denoted e or e'. The wave vectors of the three pulses are all different unless stated otherwise. For a two electronic state system, each surviving term in the perturbation series for emission in direction $\mathbf{k}_c + \mathbf{k}_b - \mathbf{k}_a$ is represented by one of the eight double-sided Feynman diagrams D_1-D_8 shown in Fig. 2 (or by a conjugate diagram terminating in the matrix element ρ_{ge} instead of

ρ_{eg} which makes a complex conjugate contribution to the signal). Rules for correspondence between terms in the perturbation series [59], and diagrams can be found in the books by Shen [49] and Mukamel [41].

At second order, linear absorption is described by two terms in the density-matrix perturbation series, and always appears in two related Feynman diagrams (plus their complex conjugates). One diagram depopulates the ground state, and leaves the photon number unchanged, while the other diagram populates the excited state and annihilates a photon. The diagrams shown above each other in Fig. 2 all have such related ''absorption pairs'' in their first two steps, and cannot occur separately. Similarly, the last indicated element of the density matrix yields an electronic polarization whose spontaneous radiation affects the final value of two diagonal density-matrix elements at fourth order. The two extensions of each diagram are *both* required to describe the simple four-wave mixing process of two incoherent, sequential linear absorption or emission steps.

Following standard usage [41], t_1, t_2, and t_3 will be used for the positive-ordered time intervals between perturbation theoretic field-matter interactions. The time between the first and second interactions is t_1; t_2 is the interval between the second and third interactions; and t_3 is the time between the third interaction and the present (t). We retain the separate unordered pulse specific interaction times τ_a, τ_b, and τ_c of the complete response because they are convenient when pulses overlap in time, and interaction order need not match nominal pulse order. Figure 1 shows a pulse sequence to illustrate the relevant time variables. The experimentally controlled maxima of the pulse envelopes are denoted t_a, t_b, and t_c. For convenience we use the standard three pulse echo time intervals $\tau \equiv t_b - t_a$ and $T \equiv t_c - \max(t_a, t_b)$.

The eight diagrams can be grouped in three ways [60]. Diagrams D_1, D_2, D_5, and D_6 involve evolution on the excited electronic state during t_2, while D_3, D_4, D_7, and D_8 evolve on the ground electronic state during t_2. The excited-state evolution can be understood as wave-packet probability density motion, while the ground-state evolution closely approximates the motion of a ''hole'' in the equilibrium probability density at high temperature [61]. Since ground-state depopulation equals excited-state population in a two-electronic-state system, ground- and excited-state diagrams usually contribute equally to degenerate four-wave-mixing signals. The second grouping is based on macroscopic rephasing phenomena. Diagrams D_2, D_3, D_6, and D_7 involve nearly conjugate density-matrix elements with opposite sign frequency evolutions during $t_1(\rho_{ge})$ and $t_3(\rho_{e'g'})$, so that they can yield a macroscopic inhomogeneous dipole rephasing (photon echo signal) when $t_3 \approx t_1$. D_1, D_4, D_5, and D_8 involve similar frequency evolutions during $t_1(\rho_{eg})$ and $t_3(\rho_{eg'})$, and cannot produce macroscopic rephasing. The third grouping is based on the order of interaction with pulses b and c. Diagrams D_1–D_4 have an interaction with pulse b before the interaction with pulse c (''properly'' time-ordered group), and represent the scattering of pulse c off a grating formed by pulses a and b. Diagrams D_5–D_8 have an interaction with pulse c before that with pulse b (''improperly'' time-ordered group) and represent the scattering of pulse b off the grating formed by pulses a and c. ''Improper'' time orderings can complicate the signal when pulses b and c overlap in time, and both sets of diagrams simultaneously contribute to the signal [60,62,63].

Since pulses b and c both contribute to the signal wave vector with positive signs, the eight diagrams shown in Fig. 2 involve only four functionally distinct density-matrix pathways. The diagrams have been numbered so that D_i and D_{i+4} have the same density-matrix pathway and sample the same microscopic dynamics, though at different times and in response to different external fields. The four distinct density-matrix pathways have microscopic response functions given by Eq. (3) in terms of time intervals between ordered interactions of the electric fields with the system. The four time-ordered response functions R_i are given by a slight generalization of Eq. (7.11) from Mukamel's monograph [41] to include electronic sublevels:

$$R_1(t_1,t_2,t_3) = \sum_{g,g',e,e'} \mu_{eg'}^* \mu_{e'g'} \mu_{e'g}^* \mu_{eg} \langle \mathcal{G}_{eg'}(t_3) \mathcal{G}_{ee'}(t_2) \mathcal{G}_{eg}(t_1) \rho_{gg} \rangle,$$

$$R_2(t_1,t_2,t_3) = \sum_{g,g',e,e'} \mu_{e'g'}^* \mu_{eg'} \mu_{e'g} \mu_{eg}^* \langle \mathcal{G}_{e'g'}(t_3) \mathcal{G}_{e'e}(t_2) \mathcal{G}_{ge}(t_1) \rho_{gg} \rangle,$$

$$R_3(t_1,t_2,t_3) = \sum_{g,g',e,e'} \mu_{e'g'}^* \mu_{e'g} \mu_{eg'} \mu_{eg}^* \langle \mathcal{G}_{e'g'}(t_3) \mathcal{G}_{gg'}(t_2) \mathcal{G}_{ge}(t_1) \rho_{gg} \rangle,$$

$$R_4(t_1,t_2,t_3) = \sum_{g,g',e,e'} \mu_{e'g}^* \mu_{e'g'} \mu_{eg'}^* \mu_{eg} \langle \mathcal{G}_{e'g}(t_3) \mathcal{G}_{g'g}(t_2) \mathcal{G}_{eg}(t_1) \rho_{gg} \rangle,$$

$$(3)$$

where μ_{eg} is the transition dipole matrix element $\langle e|\hat{\mu}|g \rangle$, ρ_{gg} is the diagonal density-matrix element $\langle g|\hat{\rho}|g \rangle$, and $\mathcal{G}_{mn}$ is the Green function for the set of density-matrix elements indicated by the subscripts. The Green functions $\mathcal{G}_{nm}$ are defined by [Mukamel's Eq. (7.5)] [41] their action on an arbitrary operator **A**:

$$\mathcal{G}_{nm}(t)\mathbf{A} = \theta(t)\exp(-i\mathbf{H}_n t/\hbar)\mathbf{A}\exp(i\mathbf{H}_m t/\hbar), \quad (4)$$

TABLE I. Connection between Feynman diagrams and response function. *For a two level-system, no diagram which survives the rotating-wave approximation is phase matched with wave vector $\mathbf{k}_{sa} = -\mathbf{k}_a + \mathbf{k}_b + \mathbf{k}_c$.

Interaction times	Diagrams	Response	t_1	t_2	t_3
$(\tau_b \geq \tau_a \geq \tau_c)$	D_1 and D_4	$R_1 + R_4$	$\tau_b - \tau_a$	$\tau_a - \tau_c$	τ_c
$(\tau_a > \tau_b \geq \tau_c)$	D_2 and D_3	$R_2 + R_3$	$\tau_a - \tau_b$	$\tau_b - \tau_c$	τ_c
$(\tau_a \geq \tau_c > \tau_b)$	D_6 and D_7	$R_2 + R_3$	$\tau_a - \tau_c$	$\tau_c - \tau_b$	τ_b
$(\tau_c > \tau_a \geq \tau_b)$	D_5 and D_8	$R_1 + R_4$	$\tau_c - \tau_a$	$\tau_a - \tau_b$	τ_b
$(\tau_c \geq \tau_b > \tau_a)$	*	0	$\tau_c - \tau_b$	$\tau_b - \tau_a$	τ_a
$(\tau_b > \tau_c > \tau_a)$	*	0	$\tau_b - \tau_c$	$\tau_c - \tau_a$	τ_a

where $\theta(t)$ is the Heaviside step function, and $\mathbf{H}_m$ is the Hamiltonian of state m. The Green functions contain a factor $\exp(-i\omega_{nm}t)$ oscillating at the Bohr frequency $\omega_{nm} = (E_n - E_m)/\hbar$. The brackets in Eq. (3) denote a full trace over both system and bath coordinates. The sums are usually taken to include an inhomogeneous ensemble average. In the optical Bloch limit, $\mathcal{G}_{nm}(t) = \theta(t)\exp(-\Gamma_{nm}t)\exp(-i\omega_{nm}t)$, where Γ_{nm} is a dephasing rate $(1/T_2)$ when $n \neq m$, or a population relaxation rate $(1/T_1)$ when $n = m$. The response function R_i can be used in calculating the polarization from the

diagram D_i (for $i = 1-4$) and, using different time arguments, D_{i-4} (for $i = 5-8$). The interaction ordering for which each diagram contributes, the response functions, and the connection between the ordered positive time intervals t_1, t_2, and t_3 and the unordered positive interaction times τ_a, τ_b, and τ_c are given in Table I for polarization wave vector $\mathbf{k}_{sa} = -\mathbf{k}_a + \mathbf{k}_b + \mathbf{k}_c$.

The complex phase-matched part $\hat{S}^{(3)}(\mathbf{k}_{sa}, \tau_a, \tau_b, \tau_c)$ of the complete third-order response function $\chi^{(3)}(\tau_a, \tau_b, \tau_c)$ is written out in Eq. (5):

$$\hat{S}^{(3)}(\mathbf{k}_{sa}, \boldsymbol{\tau}_a, \boldsymbol{\tau}_b, \boldsymbol{\tau}_c) = \begin{cases} (i/\hbar)^3 N[R_1(\tau_b - \tau_a, \tau_a - \tau_c, \tau_c) + R_4(\tau_b - \tau_a, \tau_a - \tau_c, \tau_c)] & (\tau_b \geq \tau_a \geq \tau_c) \\ (i/\hbar)^3 N[R_2(\tau_a - \tau_b, \tau_b - \tau_c, \tau_c) + R_3(\tau_a - \tau_b, \tau_b - \tau_c, \tau_c)] & (\tau_a > \tau_b \geq \tau_c) \\ (i/\hbar)^3 N[R_2(\tau_a - \tau_c, \tau_c - \tau_b, \tau_b) + R_3(\tau_a - \tau_c, \tau_c - \tau_b, \tau_b)] & (\tau_a \geq \tau_c > \tau_b) \\ (i/\hbar)^3 N[R_1(\tau_c - \tau_a, \tau_a - \tau_b, \tau_b) + R_4(\tau_c - \tau_a, \tau_a - \tau_b, \tau_b)] & (\tau_c > \tau_a \geq \tau_b) \\ 0 & (\tau_c \geq \tau_b > \tau_a) \\ 0 & (\tau_b > \tau_c > \tau_a) \end{cases}, \quad (5)$$

where N is the number density. Like $\chi^{(3)}$, the complex phase-matched response $\hat{S}^{(3)}(\mathbf{k}_{sa}, \tau_a, \tau_b, \tau_c)$ is zero for negative τ_α by causality. The response for positive τ_α is divided by three planes ($\tau_a = \tau_b$, $\tau_b = \tau_c$, and $\tau_c = \tau_a$) into six regions corresponding to the six ways to order 3 interactions. For positive τ_α, the phase-matched response has only one surface of discontinuity (the union of the plane $\tau_a = \tau_c$ for $\tau_b \geq \tau_c$, with the plane $\tau_a = \tau_b$ for $\tau_c \geq \tau_b$) where the response drops abruptly to zero when the interactions with pulses b and c both precede that with a. The discontinuity arises in the rotating-wave approximation because the only resonant grating formed by b and c in a two electronic state system has wave vector $\mathbf{k}_b - \mathbf{k}_c$ and scatters pulse a into directions $\mathbf{k}_a \pm (\mathbf{k}_b - \mathbf{k}_c)$, where it does not contribute to the signal of interest. Only four interaction orderings contribute

to a given fully noncollinear third-order polarization in a two-electronic-state system. The strength of a given time-ordered contribution to the polarization depends on the order in which the pulses reach the system, but the interaction order need not match the nominal pulse order when the pulses overlap in time.

To obtain the phase-matched polarization with wave vector, $\mathbf{k}_{sb} = \mathbf{k}_a - \mathbf{k}_b + \mathbf{k}_c$, the labels for pulses a and b are interchanged. Equation (6) gives the expression for the complex phase-matched part of the third-order response $\hat{S}^{(3)}(\mathbf{k}_{sb}, \tau_a, \tau_b, \tau_c)$ in the $\mathbf{k}_{sb}$ direction. The two orderings with b and c first do contribute to the signal with phase-matching direction, $\mathbf{k}_{sb} = \mathbf{k}_a - \mathbf{k}_b + \mathbf{k}_c$, while the two orderings with a and c first do not contribute to the signal in this direction:

$$\hat{S}^{(3)}(\mathbf{k}_{sb},\tau_a,\tau_b,\tau_c) = \begin{cases} (i/\hbar)^3 N[R_2(\tau_b-\tau_a,\tau_a-\tau_c,\tau_c)+R_3(\tau_b-\tau_a,\tau_a-\tau_c,\tau_c)] & (\tau_b>\tau_a\geq\tau_c) \\ (i/\hbar)^3 N[R_1(\tau_a-\tau_b,\tau_b-\tau_c,\tau_c)+R_4(\tau_a-\tau_b,\tau_b-\tau_c,\tau_c)] & (\tau_a\geq\tau_b\geq\tau_c) \\ 0 & (\tau_a\geq\tau_c>\tau_b) \\ 0 & (\tau_c>\tau_a>\tau_b) \\ (i/\hbar)^3 N[R_1(\tau_c-\tau_b,\tau_b-\tau_a,\tau_a)+R_4(\tau_c-\tau_b,\tau_b-\tau_a,\tau_a)] & (\tau_c>\tau_b\geq\tau_a) \\ (i/\hbar)^3 N[R_2(\tau_b-\tau_c,\tau_c-\tau_a,\tau_a)+R_3(\tau_b-\tau_c,\tau_c-\tau_a,\tau_a)] & (\tau_b\geq\tau_c>\tau_a). \end{cases} \tag{6}$$

The nonlinear polarization with wave vector $\mathbf{k}_s$ is given by a triple convolution over the complex phase-matched part of the third-order response $\hat{S}^{(3)}(\mathbf{k}_s,\tau_a,\tau_b,\tau_c)$:

$$P^{(3)}(\mathbf{k}_{sa},t) = \int_0^\infty \int_0^\infty \int_0^\infty \hat{S}^{(3)}(\mathbf{k}_{sa},\tau_a,\tau_b,\tau_c)\hat{E}_a^*(t-\tau_a)$$
$$\times \hat{E}_b(t-\tau_b)\hat{E}_c(t-\tau_c)d\tau_a d\tau_b d\tau_c + \text{c.c.}. \tag{7}$$

The form of delayed pulses must match the experiment to calculate the phase of the nonlinear polarization. The electric fields used here are of the envelope delayed form generated by an interferometer path difference (i.e., the maxima of the field oscillations always occur at the same times relative to the maximum of the field envelope) [38]. The complex electric fields are given by $\hat{E}_\alpha(t)=\hat{e}(t-t_\alpha)\exp[-i\omega_\alpha(t-t_\alpha)]$, where $\alpha=a$, b, c, and t_α represents the delay of pulse α (so that pulses a, b, and c are centered at times t_a, t_b, and t_c, respectively). The complex envelope $\hat{e}(t)=e(t)\exp[i(\omega_\alpha t - \phi(t))]$, where $e(t)$ is the real envelope defined below Eq. (1), allows the inclusion of chirp or phase shifts. The origin of time is set at the center of pulse c ($t_c=0$). When the explicit complex time-domain fields are inserted into Eq. (7), we obtain

$$P^{(3)}(\mathbf{k}_{sa},t,t_a,t_b) = \int_0^\infty \int_0^\infty \int_0^\infty \hat{S}^{(3)}(\mathbf{k}_{sa},\tau_a,\tau_b,\tau_c)$$
$$\times \hat{e}_a^*(t-t_a-\tau_a)\hat{e}_b(t-t_b-\tau_b)\hat{e}_c(t-\tau_c)$$
$$\times \exp[i\omega_a(t-t_a-\tau_a)]$$
$$\times \exp[-i\omega_b(t-t_b-\tau_b)]$$
$$\times \exp[-i\omega_c(t-\tau_c)]d\tau_a d\tau_b d\tau_c + \text{c.c.} \tag{8}$$

Restricting $e'=e$ and $g'=g$, Eq. (8) differs from earlier treatments of noncollinear three-pulse scattering based on the same formalism [51,60] only by a constant phase (i^3) and the use of envelope pulse delays. The third-order polarization with wave vector $\mathbf{k}_{sb}=\mathbf{k}_c-\mathbf{k}_b+\mathbf{k}_a$ is given by

$$P^{(3)}(\mathbf{k}_{sb},t,t_a,t_b) = \int_0^\infty \int_0^\infty \int_0^\infty \hat{S}^{(3)}(\mathbf{k}_{sb},\tau_a,\tau_b,\tau_c)$$
$$\times \hat{e}_a(t-t_a-\tau_a)\hat{e}_b^*(t-t_b-\tau_b)\hat{e}_c(t-\tau_c)$$
$$\times \exp[-i\omega_a(t-t_a-\tau_a)]$$
$$\times \exp[+i\omega_b(t-t_b-\tau_b)]$$
$$\times \exp[-i\omega_c(t-\tau_c)]d\tau_a d\tau_b d\tau_c + \text{c.c.}. \tag{9}$$

Pulse-pair pump-probe measurements (sometimes referred to as heterodyne-detected phase-locked pump-probe) were proposed [42] as an alternate way to characterize relaxation processes with memory (e.g., solvation) and measured in Refs. [43], [64]. In pulse-pair pump-probe measurement the pump ''pulse'' is a collinear pulse pair, with pulse pair delay τ, and the probe, which arrives at time T after the second pulse in the pulse pair, is noncollinear. In a noncollinear three-pulse scattering experiment, the signal energy can be an asymmetric function of τ, but the signals in the $\mathbf{k}_{sa}$ and $\mathbf{k}_{sb}$ directions are mirror images of each other about $\tau=0$. The partly collinear pulse-pair pump-probe experiment superimposes these two signal fields. Two pump-probe fields (one excited by each pulse in the pulse pair with the probe pulse) are also radiated in the same direction as the pulse-pair pump-probe field, and must be subtracted to obtain the pulse-pair pump-probe signal [43]. The modulation of the spectrum of the pulse pair causes an amplitude modulation of the probe at the initial dipole frequency ω_{eg} as a function of the delay τ between the pump pulses. The pump-probe signals generated by a single pulse in the pump pulse pair do not contribute to the modulation in the signal, which is entirely due to the three-pulse contributions. Phase matching dictates that the signal field will be emitted along the wave vector of the third excitation pulse ($\mathbf{k}_s=\mathbf{k}_{sa}=\mathbf{k}_{sb}=\mathbf{k}_c$). When pulses a and b are collinear, the part of the third-order polarization with wave vector $\mathbf{k}_s=\mathbf{k}_c$ that depends on all three excitation fields is given by

$$P^{(3)}_{abc}(\mathbf{k}_c,t,t_a,t_b) = P^{(3)}(\mathbf{k}_{sa},t,t_a,t_b)+P^{(3)}(\mathbf{k}_{sb},t,t_a,t_b). \tag{10}$$

The subscript abc on $P^{(3)}_{abc}(\mathbf{k}_c)$ indicates that contributions to the nonlinear polarization which do not depend on all three pulses are excluded.

We now turn to the phase of the polarization. At first order ($\chi^{(1)}$ process), each pulse excites dipoles which then radiate freely (free-induction decay or FID) in the same direction. For positive ω_{eg} (absorption), the dipoles lag the excitation field by $\pi/2$ at exact resonance [65]. For an infinite plane wave, the freely radiated field lags the source polarization by $\pi/2$ for each frequency component [66]. Resonant components of the linear FID are thus π out of phase with the excitation field, and interfere destructively with it, causing absorption [65]. In centrosymmetric media, the next nonzero responses are third-order nonlinear responses ($\chi^{(3)}$ process) to all combinations of the input pulses [49]. For a two-electronic-state system, a three-pulse experiment produces three saturated free-induction decays, six pump-probe signals, six self-diffraction signals, and three three-pulse scattering signals. When all three perturbation theoretic interactions involve the same pulse, the i^3 phase factor in Eqs. (5) and (6) indicates that the third-order nonlinear polarization lags the pulse by $3\pi/2$ at exact resonance when ω_{eg} is positive. As in the linear case, the phase between the third-order polarization and the exciting field depends on detuning. The resonant third-order polarization is π out of phase with the linear polarization (saturated FID), and radiates in phase with the excitation field, leading to reduced or saturated absorption. Any combination of two pulses excites a third-order polarization in which one pulse formally interacts twice and the other once. The use of two formal interactions with pulse a to bleach the absorption seen by pulse c through excitation of a nonlinear polarization with wave vector $\mathbf{k}_s = \mathbf{k}_c + \mathbf{k}_a - \mathbf{k}_a$ is one of the six pump-probe signals. This increased probe transmission is called a positive pump-probe signal here. Two-pulse self-diffraction signals [19] (e.g., two pulse echoes [41]) can be detected in background-free directions such as $\mathbf{k}_s = 2\mathbf{k}_b - \mathbf{k}_a$. In three-pulse scattering, three identical pulses with different wave vectors each formally interact once, and signals of approximately the same frequency are emitted in the directions $\mathbf{k}_{sa}$, $\mathbf{k}_{sb}$, and $\mathbf{k}_{sc} = \mathbf{k}_a + \mathbf{k}_b - \mathbf{k}_c$. Setting $\tau = 0$ and $\phi_b = \phi_a$, so that the first two pulses are identical and coincident on the sample, the i^3 phase factor indicates that the nonlinear polarization lags pulse c by $3\pi/2$ at exact resonance when ω_{eg} is positive. In general, a change in the sign of ω_{nm} can introduce a π phase shift corresponding to a distinction between absorption and emission. This phase is always the same when all population starts in the lower state of a two electronic state system, and will not be considered further.

The microscopic factors contributing to the phase of the third-order nonlinear polarization are now introduced. If the excitation pulses a, b, and c are phase shifted by ϕ_a, ϕ_b, and ϕ_c, respectively, the nonlinear polarization with wave vector $\mathbf{k}_{sa} = \mathbf{k}_c + \mathbf{k}_b - \mathbf{k}_a$ is phase shifted by $(\phi_c + \phi_b - \phi_a)$ [38,41,42]. In general, constant spectral phase shifts ϕ_α of the excitation pulses produce a constant spectral phase shift $\phi_s = \Sigma s_\alpha \phi_\alpha$ of the nonlinear polarization with wave vector $\mathbf{k}_s = \Sigma s_\alpha \mathbf{k}_\alpha$ (where $s_\alpha = \pm 1$ and $\alpha = a, b, c$). Polarizers and waveplates can accurately approximate constant spectral phase shifts over narrow spectral regions, and have been used to phase shift the signal and/or local oscillator in picosecond polarization spectroscopy [67,68]. A similar phase

shift is used in magnetic resonance for isolating the signal of interest [69,70].

There is also a term in the phase arising from dipole oscillation during τ. Setting $\omega_0 = \omega_a = \omega_b = \omega_c$ and examining the complex integral in Eq. (8), the resonant field oscillates as $\exp[-i\omega_0(\tau_a - \tau_b - \tau_c)]$. Combining Eqs. (3), (4), and (5), it can be seen that the response function $\hat{S}^{(3)}$ oscillates as $\exp[i\omega_{eg}(\tau_a - \tau_b)]\exp[-i\omega_{e'g'}\tau_c]$, approximately canceling the resonant field oscillations in Eq. (8) and leaving only a slowly oscillating term. (This is strictly true only for the properly ordered response. Since the improperly ordered response contributes only when pulses b and c overlap, an approximate swap between τ_b and τ_c in the improperly ordered response is used for this discussion.) This cancellation was enforced by the rotating-wave approximation from the beginning. However, the resonant field oscillations with the delays t_a and t_b are not approximately canceled, and $\exp[i\omega_0(t_b - t_a)]$ can be pulled outside the integral along with $\exp[-i(\omega_c + \omega_b - \omega_a)t] = \exp[-i\omega_0 t]$. For transform-limited pulses, the effect of the slowly oscillating term left by the rotating-wave approximation can be approximated using $\tau_a \approx t - t_a$, $\tau_b \approx t - t_b$, and $\tau_c \approx t$ (Fig. 1), and combined with the field oscillations to yield $\exp[i\omega_{eg}(t_b - t_a)]\exp[-i\omega_{e'g'}t]$. With the definition $\tau \equiv (t_b - t_a)$, the component of the nonlinear polarization $P^{(3)}(\mathbf{k}_{sa})$ radiating at frequency $\omega_{e'g'}$ has a pulse-delay-dependent phase modulation $-\omega_{eg}\tau$. When discussing the τ-dependent phase of a polarization which changes temporal shape with τ, it is convenient to reference the phase to that of the last pulse (c) at $t = 0$, so that the phase of $P^{(3)}(\mathbf{k}_{sa})$ is $\phi_{sa} - \phi_c = -\omega_{eg}\tau + (\phi_b - \phi_a)$. An entirely similar analysis of the noncollinear third order polarization $P^{(3)}(\mathbf{k}_{sb})$ with wave vector $\mathbf{k}_{sb} = \mathbf{k}_c - \mathbf{k}_b + \mathbf{k}_a$, given by Eq. (9), indicates that the phase is $\phi_{sb} - \phi_c = +\omega_{eg}\tau - (\phi_b - \phi_a)$. The two phase shifts are exactly equal and opposite because the scattered signal fields are equal and opposite orders of diffraction off the grating formed by pulses a and b. If the experiment employs carrier-wave-delayed pulses (which can be generated by acousto-optic modulation of a continuous-wave laser [46] or frequency-domain phase control methods [71]), $\omega_{eg}\tau$ should be replaced by $(\omega_{eg} - \omega_0)\tau$, where ω_0 is the carrier frequency.

The product of four transition dipoles in the response function [Eq. (3)] also contributes a variable phase factor to the signal, mentioned briefly by Mitsunaga, Kintzer, and Brewer [45]. Two demonstrations that this phase can only be 0 or π will be given. The first demonstration applies if an even number of transition moments of the same type (e.g., four electric dipole transitions or four magnetic dipole transitions) form a closed cycle. Feynman energy ladder subdiagrams [40] showing four different sublevels involved in the sums in Eq. (3) are useful (Fig. 3). The transition dipole products can all be rearranged into the following form:

$$\langle g|\mu|e\rangle\langle e|\mu|g'\rangle\langle g'|\mu|e'\rangle\langle e'|\mu|g\rangle. \qquad (11)$$

This expression is invariant to the arbitrary phase factors chosen for any $|\psi\rangle$. Defining $|\alpha\rangle = \mu|e\rangle$ and $|\beta\rangle = \mu|e'\rangle$, Eq. (11) becomes $\langle g|\alpha\rangle\langle\alpha|g'\rangle\langle g'|\beta\rangle\langle\beta|g\rangle$. Recognizing that the product of projection operators $|\alpha\rangle\langle\alpha\|g'\rangle\langle g'\|\beta\rangle\langle\beta|$ is a
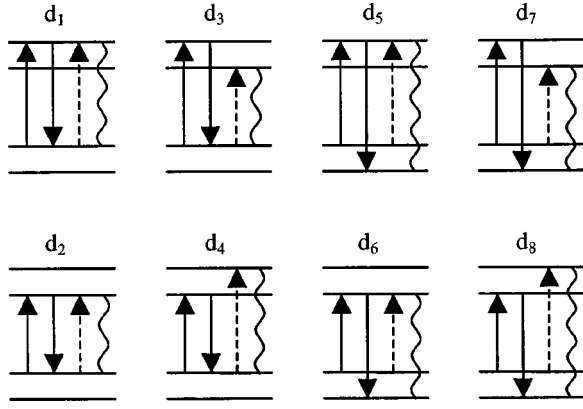
FIG. 3. Some energy ladder Feynman subdiagrams represented by the double-sided Feynman diagram D_3 for a system with two sublevels in each electronic state. There are 16 energy ladder subdiagrams for every double-sided diagram in Fig. 2. Of the 16 subdiagrams for D_3, only the eight beginning in the upper sublevel of the ground state are shown. Time runs from left to right with field-matter interactions in the order a, b, and c. The wavy line on the right indicates the radiating polarization. Subdiagrams d_1 and d_2 represent ground-state bleaching of the initially excited transition, while subdiagrams d_3 and d_4 represent V-type double resonances. Subdiagrams d_5-d_8 all represent resonant stimulated Raman processes. Note that only subdiagrams d_7 and d_8 involve all four levels and four different transition dipole matrix elements. Subdiagram d_8 can radiate outside the spectrum of the excitation pulses. The other eight subdiagrams originating in the other sublevel can be grouped in the same way, and a similar grouping holds for the 16 energy ladder subdiagrams belonging to all eight double-sided diagrams.

projection operator and hence Hermitian, the product of transition moments must be real. If only three levels are involved (e.g., subdiagrams d_1-d_6 in Fig. 3: V- or Λ-type double resonances in optics; [72] regressively connected transitions of order $q=0$ in NMR [70]), the product can be rewritten as $\mu_{ab}\mu_{ab}^*\mu_{bc}\mu_{bc}^*$ and must be real and positive or zero. Negative real products, which are possible for subdiagrams d_7 and d_8 in Fig. 3, were first observed for four-level transitions in strongly coupled ABX spin systems by two-dimensional Fourier transform magnetic resonance [73]. These four-level four-wave-mixing transitions will be called ''parallel'' by analogy to magnetic resonance (they are designated parallel to order $q=1$ in NMR [70]). In nonlinear optics, vibration-electronic four-level signals have been known as coherent anti-Stokes Raman scattering (CARS) or coherent Stokes Raman scattering (CSRS) [40,49], and some known four-level signals (e.g., subdiagram d_7 in Fig. 3) require three excitation frequencies [74,75]. The product of transition dipoles in Eq. (11) is real and negative for a four-level transition involving the $v=0$ and 1 levels of two electronic states with slightly displaced but otherwise identical harmonic potentials.

The above discussion assumes that the four transitions are connected in a closed cycle as in Fig. 3. In the presence of relaxation processes that transfer [76,77] or generate coherence [78,79], a closed-cycle connection may not hold, and the above demonstration that the transition dipole product is real breaks down. If the Hamiltonian is invariant under time

reversal, it may be taken to be real and orthogonal with real eigenfunctions [80]. (The reality of the eigenfunctions was used by Armstrong *et al.* to calculate the phase of nonlinear optical signals generated by monochromatic sources [39].) Since this implies each transition dipole matrix element may be taken as real, the transition dipole product is real even in the presence of relaxation generated coherence. This time-reversal demonstration does not apply to magnetic resonance because the external magnetic field breaks time reversal.

Finally, the emitted field is phase shifted relative to the polarization. The nonlinear polarization acts as a source of spontaneously emitted electromagnetic radiation in Maxwell's equations [41,49]. The second-order differential equation connecting the polarization to the electric field [Eq. 3.21(a) of Shen [49]] is *linear* in both the electric field and the nonlinear polarization (if we ignore the field dependence of the source polarization). A Fourier decomposition into complex frequency-domain electric fields and source polarizations is therefore possible. $\hat{E}_{\mathrm{sig}}(\omega) \equiv \int_{-\infty}^{\infty} E_{\mathrm{sig}}(t) \exp(i\omega t)dt$ and $\hat{P}^{(3)}(\omega)$ are defined as the inverse Fourier transforms of $E_{\mathrm{sig}}(t)$ and $P^{(3)}(t)$. The infinite plane wave and negligible pump depletion approximations give $\hat{E}_\alpha(\omega, \vec{r}) = \hat{E}_\alpha(\omega, 0)\exp(i\vec{k}_\alpha \cdot \vec{r})$, $\alpha = a, b, c$ [49]. Assuming slow changes in complex spectral amplitude $\hat{e}_{\mathrm{sig}}(\omega, z) \equiv \hat{E}_{\mathrm{sig}}(\omega, z)\exp(-ikz)$ over a wavelength, $|\partial^2 \hat{e}_{\mathrm{sig}}(\omega, z)/\partial z^2| \ll |k\partial \hat{e}_{\mathrm{sig}}(\omega, z)/\partial z|$ (slowly evolving wave approximation [54]) then yields the field at the sample exit:

$$\hat{E}_{\mathrm{sig}}(\omega) = \frac{2\pi l}{n(\omega)c} i\omega \hat{P}^{(3)}(\omega) \mathrm{sinc}(\Delta kl/2)\exp(i\Delta kl/2).$$

$$(12)$$

The proportionality of the spontaneously emitted field to ω (charge velocity) rather than ω^2 (charge acceleration) results from the infinite plane-wave approximation [66]. This spontaneous radiation factor has been included in two recent treatments of second-harmonic frequency-resolved optical gating [25,26]. (In the treatment of Ref. [26], the infinite plane-wave result was multiplied by an additional frequency factor arising from diffraction limited focal spot size dependence on wavelength [81]. The complex space-time evolution [54,82] of four-wave-mixing signals with focused beams is not treated here.) Imperfect phase matching can lead to phase shifts of the signal [e.g., the $\exp(i\Delta kl/2)$ factor above], and complex interactions between propagating phase-mismatched signal and excitation pulses have been studied through their effect on the signal energy [83]. Perfect phase matching ($\Delta kl=0$) will be assumed, so that these complexities disappear. For narrowband pulses, ω may be approximated as constant [$\omega = \omega_0 \mathrm{sgn}(\omega)$], and Eq. (12) indicates that the emitted signal field lags $\pi/2$ behind the nonlinear source polarization. Ignoring the frequency dependence of the refractive index $n(\omega)$ (which is reasonable for dilute chromophores in transparent media if the pulse spectrum is not too wide), Eq. (12) becomes the Fourier transform of a derivative, to yield

$$E_{\mathrm{sig}}(t) \cong -\frac{2\pi l}{nc}\frac{dP^{(3)}(t)}{dt},$$

$$(13)$$

where l is the length of the sample, n is the refractive index of the medium, c is the speed of light in vacuum, and $P^{(3)}(t)$ is given by Eq. (8), (9), or (10). Equation (13) can be used to calculate the signal electric field from the third-order nonlinear polarization.

For a two-level system in the optical Bloch limit, the nonlinear polarization can be explicitly calculated for δ function pulses [84]. For $t \geq 0$, the signal field is given by

$$E(t,\tau,T) = \frac{2\pi l}{nc}(\Gamma^2 + \omega_{eg}^2)^{1/2}\exp[-\Gamma(t+|\tau|)]$$
$$\times \exp(-T/T_1)\cos[\omega_{eg}(t-\tau)+\phi]$$
$$\times [1-(1/2)\delta(T)\theta(-\tau)], \qquad (14)$$

where ω_{eg} is the (positive) electronic transition frequency, Γ is the dipole decay rate ($1/T_2$), T_1 is the population grating lifetime, and $\phi = \arctan(\Gamma/\omega_{eg})$ is an extra emission phase shift. No signal is emitted before $t=0$. For $T=0$, a discontinuity in the signal field occurs at $\tau=0$, where the field jumps by a factor of 2 for positive τ. Mathematically, pulses straddle the discontinuity in $S^{(3)}$ at $\tau_a = \tau_c$ for negative τ (which reduces the signal by a factor of 2), while pulses straddle the continuous proper-improper boundary at $\tau_b = \tau_c$ for positive τ. Physically, scattering pulse b off a grating that is halfway formed by a and c compensates for the half-complete formation of the ab grating at $T=0$ only for positive τ. Equation (14) differs from Eq. (1) given by Hybl *et al.* (which was valid only for $T>0$) because the time derivative of the polarization is used to obtain the field (instead of an approximate $\pi/2$ phase shift). The polarization emission yields an additional phase shift $\arctan(\Gamma/\omega_{eg})$ of the emitted field through the decay of the nonlinear polarization envelope. In the case of large Gaussian inhomogeneous broadening [center ω_0, full width at half maximum $\sqrt{8\ln(2)}\sigma$], the emitted field has a time-dependent amplitude change and emission phase shift $\phi(t) = \arctan[\sigma^2(t-\tau)/\omega_0]$. The apparent complexity of the radiated field suggests that $\hat{P}^{(3)}(\omega)$ obtained from the inverse Fourier transform of the field using Eq. (12) may be more useful for microscopically oriented investigations. In the following numerical calculations, the ''pseudofield''

$$F(t) = \frac{1}{2\pi}\int_{-\infty}^{\infty} i\,\text{sgn}(\omega)\hat{P}^{(3)}(\omega)\exp(-i\omega t)d\omega \quad (15)$$

is used to remove the time-dependent amplitude and phase shifts caused by polarization radiation.

III. CALCULATIONS

All calculations were done on Intel-based 300-MHz personal computers using Microsoft Fortran 4.0. The algorithm for the triple convolution was based on code generously provided by Dr. Jae-Young Yu, which was modified to compute the triple integrals in Eq. (8) while fully exploiting the rotating-wave approximation. For noncollinear excitation pulses, $P^{(3)}(\mathbf{k}_{sa})$ was calculated from Eq. (8), and

$P^{(3)}(\mathbf{k}_{sb})$ was calculated from Eq. (9). For excitation by collinear pulses a and b, the three pulse nonlinear polarization $P^{(3)}_{abc}(\mathbf{k}_c)$ was calculated from Eq. (10). The excitation pulses had Gaussian envelopes $e(t) = e_0\exp(-2\ln[2]t^2/t_p^2)$ with intensity full width at half maximum t_p and transform limited temporal phase $\phi(t) = \omega_\alpha t$ with carrier frequency ω_α ($\alpha = a,b,c$). The response functions R_i were given by Eq. (8.15) in Mukamel's monograph [41] with the line-shape function $g(t)$ given by Eq. (A2) in the Appendix. The integrals over τ_a, τ_b, and τ_c were computed using the Gauss-Legendre quadrature routine GAULEG.F [85]. The interaction times τ_α in the triple integrals ranged over $(t-t_\alpha)\pm 2.5t_p$, where t_p is the Gaussian pulse duration. For most calculations, six quadrature points for each integral were enough for convergence to better than the accuracy limit imposed by the $\pm 2.5t_p$ range. To check the algorithm and code, several signals were calculated and compared to published results [60,64,86] (for details, see Ref. [87]).

Figure 4 shows surface plots of the calculated signal pseudofields $F_{\text{sig}}(t)$ (left column) and pseudo-field-envelopes $f_{\text{sig}}(t)$ (right column) as a function of t for many values of τ at four fixed values of T. The system is a Gaussian oscillator [$M(t) = \exp(-t^2/\tau_g^2)$] with $\tau_g = 100$ fs, $(\lambda/2\pi c) = 600$ cm^{-1}, and $(\omega_{eg}/2\pi c) = 1000$ cm^{-1}. Δ was set using the high temperature relation $\Delta^2 = 2\lambda k_B T/\hbar$ at temperature of 298 K. The frequency ω_{eg} and reorganization energy λ were chosen to yield only a few oscillations of the signal field for ease of visualization. The calculation used nearly impulsive pulses ($t_p = 0.1$ fs), so the signal is zero for $t<0$ and reflects the impulse response. Signal fields are shown for $T=0$, 1 fs, 50 fs, and 1 ps. In all four panels, $F_{\text{sig}}(t)$ oscillates in both the t and τ dimensions. The variation in the phase of the oscillations in both t and τ encodes the transition frequency onto the signal even after the initial coherence has decayed. The phase referenced to $t=0$ varies with τ approximately as ω_{eg}. A Fourier transform of these signals with respect to τ leads to peaks centered at the absorption frequency $\pm(\omega_{eg}+\lambda)$.

At $T=0$ [Fig. 4(a)], when the pulse duration is longer than the population time T, there is a sharp twofold rise in the calculated field and field envelope at $\tau=0$. As in the Bloch model [Eq. (14)], this jump disappears at $T=1$ fs [Fig. 4(b)], when the pulses no longer overlap. For $T=0$ and 1 fs, the emitted signal can be characterized as a stimulated photon echo: for a given value of τ, the maximum in the signal as a function of t occurs as an echo at $t=\tau$ [4,5,88]. This variation of signal emission time with τ is the signature of an effectively inhomogeneous rephasing process. At $T=50$ fs [Fig. 4(c)], there is still some movement of the signal envelope $f_{\text{sig}}(t)$ with τ, but by $T=1$ ps [Fig. 4(d)] the signal envelope's shape does not vary with τ and the signal is more properly characterized as three-pulse scattering.

Figure 5 shows the same calculation with 20-fs pulses for $T=0$ [Fig. 5(a)], $T=50$ fs [Fig. 5(b)], and $T=1$ ps [Fig. 5(c)]. The differences between the signals calculated with impulsive pulses and the signals calculated with finite bandwidth pulses is their extent in time and the displacement of the peak of the signals in the τ dimension. The finite band-
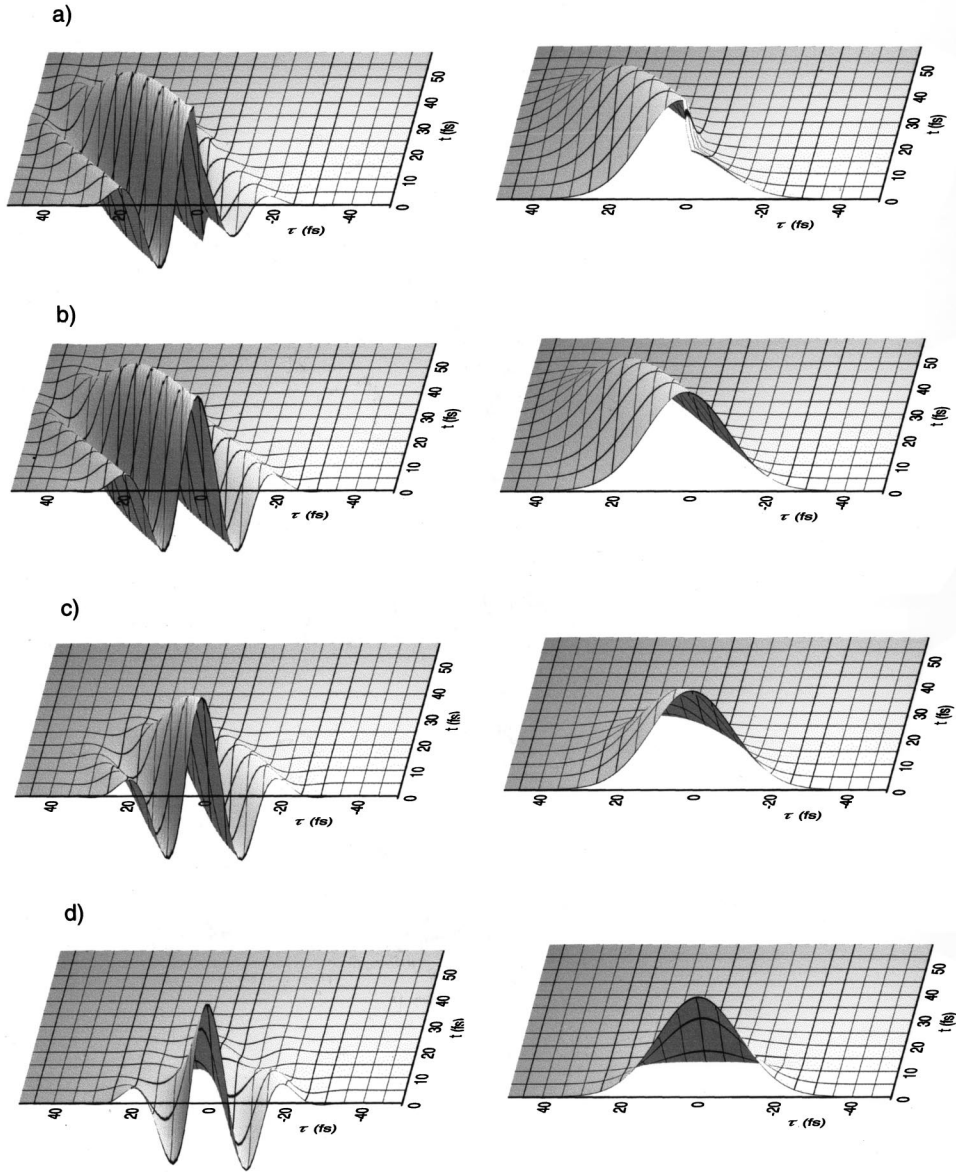
FIG. 4. Signal fields and field envelopes calculated with impulsive pulses [the intensity full width at half maximum (FWHM) is 0.1 fs] for $T=0$ (a), 1 fs (b), 50 fs (c), and 1 ps (d) for a Gaussian oscillator with time constant $\tau_g = 100$ fs. Each field and field envelope has been normalized so that each of the signals peaks at the same value. The phase modulation in the signal is such that a slice along either the t or τ axis yields a signal that oscillates near the Bohr transition frequency ($\omega_{eg} = 1000 \, \text{cm}^{-1}$). The discontinuity in the signal at $\tau=0$ is present only when the excitation pulses overlap. At $T=0$ and $T=1$ fs the signal displays "echo" behavior; the time of maximum signal envelope $e(t)$ changes with τ. At $T=50$ fs, the time of maximum signal envelope stills shows some τ dependence; by $T=1$ ps the signal envelope maximum is independent of τ and peaked at $t=0$. For $T=0$, 1 fs and 50 fs, the maximum integrated signal energy occurs at $\tau>0$ (i.e., a peak shift is observed), while for $T=1$ ps the field peaks at $t=0$ for all τ.

width signals persist longer in both the t and τ dimensions. The three pulse echo "peak shift" (value of τ with maximum signal energy integrated over t) [5,60] to positive τ is larger for longer pulses, but has decayed to zero by $T=1$ ps for both impulsive and 20-fs pulses. For $T=0$, the sharp rise observed at $\tau=0$ for δ-function pulses has become a derivative discontinuity consistent with the switch from scanning pulse b (negative τ) to scanning pulse a (positive τ) at $\tau=0$. This derivative discontinuity is also evident in the calculations shown in Fig. 7(a) of Ref. [60]. Figure 3 of Ref. [89] shows experimental evidence for a three-pulse echo derivative discontinuity at $\tau=0$.

Figure 6 shows the signal fields and envelopes for signals measured in the $\mathbf{k}_{sa}$ and $\mathbf{k}_{sb}$ directions of a noncollinear experiment, and the signal field and envelope of a pulse-pair pump-probe signal (the probe field and FID are not included). In pulse-pair pump-probe measurements the three-pulse signal is a sum of the two oppositely phase-modulated noncollinear signals in the directions $\mathbf{k}_{sa}$ and $\mathbf{k}_{sb}$. The signals shown were calculated at $T=1$ fs with impulsive pulses ($t_p = 0.1$ fs) for the Gaussian oscillator used in Figs. 4 and 5. The fields emitted in the $\mathbf{k}_{sa}$ and $\mathbf{k}_{sb}$ directions are mirror images of each other about $\tau=0$. Each is phase modulated but not amplitude modulated. In the pulse-pair pump-probe
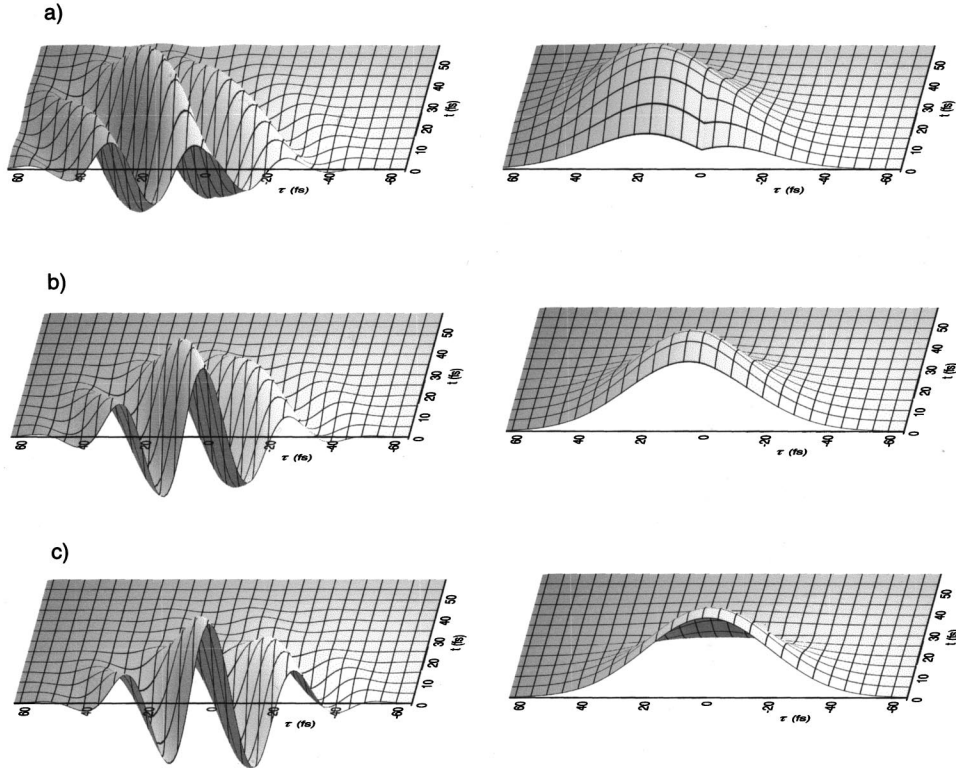
FIG. 5. Signal fields and field envelopes calculated from a Gaussian oscillator with time constant $\tau_g = 100$ fs, with 20-fs intensity FWHM pulses for $T = 0$ fs (a), 50 fs (b), and 1 ps (c). The discontinuity at $T = 0$ and $\tau = 0$ for δ-function pulses in Fig. 4 becomes a derivative discontinuity for finite bandwidth pulses. This derivative discontinuity appears only when the second and third excitation pulses overlap in time (the pulse duration is greater than population period T). The echolike behavior of the signal envelope for small T has been obscured, but is manifest in the signal maxima at positive t. With 20-fs pulses the peak shift is larger than for impulsive excitation at $T = 0$ and 50 fs, but has again decayed by $T = 1$ ps. The phase modulation is essentially unaffected by the pulse duration.

configuration ($\mathbf{k}_{sa} = \mathbf{k}_{sb}$), the interference between the $\mathbf{k}_{sa}$ and $\mathbf{k}_{sb}$ signal fields produces a signal that is amplitude modulated as well as phase modulated. The sum of these two oppositely phase modulated fields produces amplitude modulation when the two fields overlap in time. The pulse-pair pump-probe field contains time intervals when amplitude modulation dominates ($t \approx 0$ and $\tau \approx 0$) *and* intervals when phase modulation dominates ($t \approx |\tau| > 0$). The amplitude modulation has full constructive interference at $\tau = 0$, and persists well outside the δ-function pulse overlap at $\tau = 0$ but does not extend over all t [90]. If the sum of the emitted field and the third (probe) pulse is frequency resolved [32], the in-phase (absorptive/emissive) components of this signal field can be selectively detected.

IV. DISCUSSION

Measurements of the phase shift of a third-order nonlinear signal relative to the excitation pulses can be used to completely characterize the third-order nonlinear response because the unknown absolute phase common to all pulses cancels out [35]. Phase control and phase-resolved measurements thus open up new directions in nonlinear optics. The systematic treatment of the phase of nonlinear optical signals given here provides a theoretical foundation for such explorations in resonant four-wave mixing.

The use of excitation pulse phase to control the phase of the signal has been exploited to isolate desired signals in a few nonlinear optical experiments [46,91]. Strategies for systematic isolation of high-order nonlinear signals of interest by phase cycling the excitation pulses and receiver phase are well developed in magnetic resonance [69,70]. Implementation of these strategies with broadband pulses requires generation of constant spectral phase shifts by acousto-optic diffraction or frequency-domain phase shifting of individual Fourier components.

For broadband pulses, the spontaneous radiation of the nonlinear polarization produces a field that is not a simple $\pi/2$ phase-shifted version of the nonlinear polarization. The slowly evolving wave approximation used to obtain the spontaneous radiation phase shift is surprisingly accurate for pulses as short as one optical cycle [54]. For a Lorentzian line, the spontaneous radiation produces an extra constant time-domain phase shift detectable only by measuring the phase shift relative to the excitation pulses at the sample (e.g., using the method outlined by Gallagher *et al.* [35] with optics held to tolerances sufficient to eliminate constant phase differences [38]). For an inhomogeneously broadened sample, the radiation produces a signal chirp which is measurable by frequency-resolved optical gating or other implementations of spectral interferometry. For perfect phase matching, Eq. (12) can be used to remove complex radiation
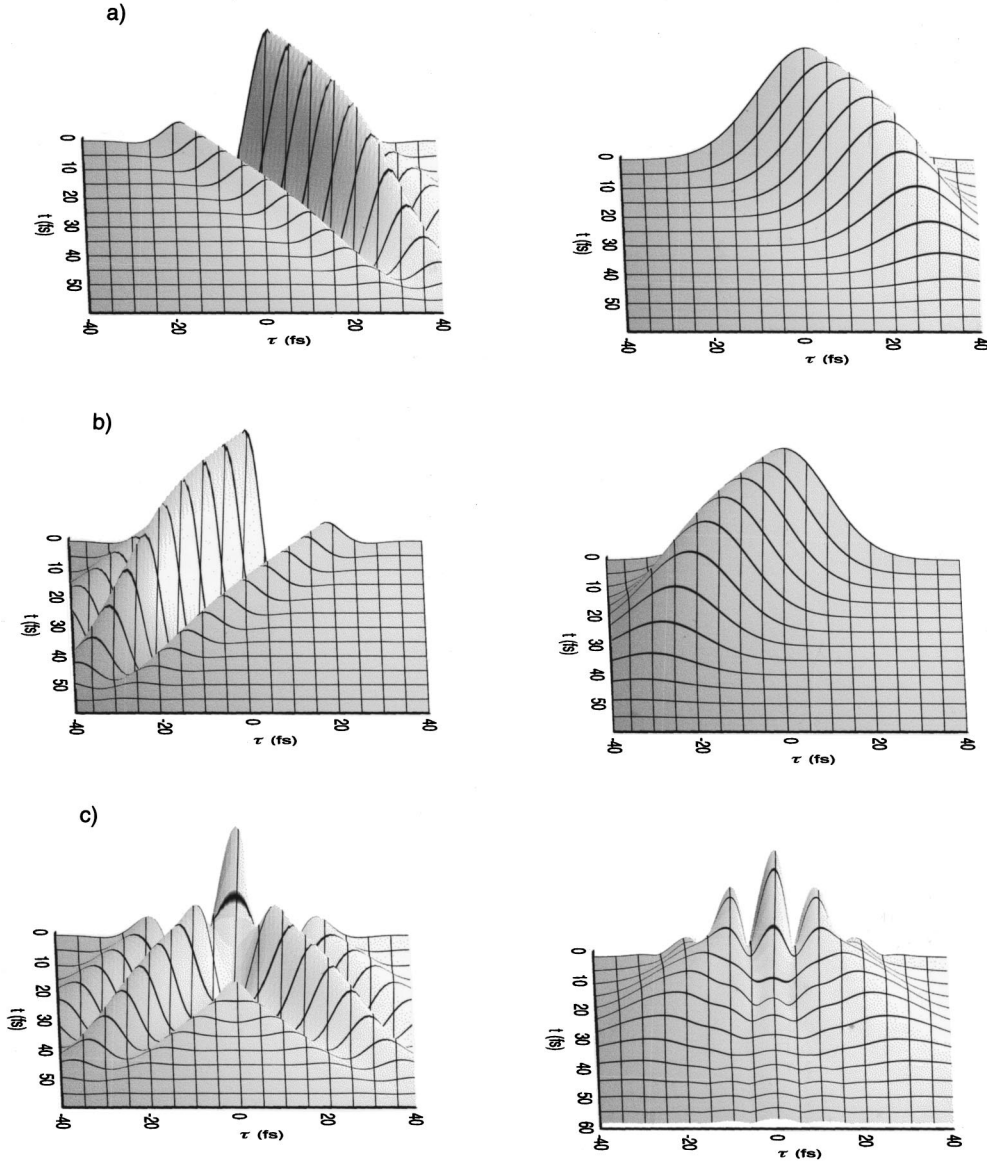
FIG. 6. Signal fields and envelopes for the two noncollinear phase-matching geometries: $\mathbf{k}_{sa} = -\mathbf{k}_a + \mathbf{k}_b + \mathbf{k}_c$ (a) and $\mathbf{k}_{sb} = \mathbf{k}_a - \mathbf{k}_b + \mathbf{k}_c$ (b), and the pulse-pair pump-probe geometry $\mathbf{k}_{sa} = \mathbf{k}_{sb}$ (c). For the $\mathbf{k}_{sa}$ noncollinear geometry, the initial value of the signal field at $t=0$ is cosinusoidally modulated at the initial dipole oscillation frequency as $-\omega_{eg}\tau$ (phase modulation), but the envelope varies smoothly with τ (no amplitude modulation). For the noncollinear $\mathbf{k}_{sb}$ signal, the phase of the signal field is modulated as $\omega_{eg}\tau$ in a counter-rotating sense to the $\mathbf{k}_{sa}$ signal field. By collapsing the fields emitted in the $\mathbf{k}_{sa}$ and $\mathbf{k}_{sb}$ directions onto each other in a partially collinear geometry with $\mathbf{k}_a = \mathbf{k}_b \neq \mathbf{k}_c$ with signal wave vector $\mathbf{k}_c$, the signal field becomes amplitude modulated when the countermodulated signals overlap in time, and phase modulated when they do not. Amplitude modulation at the initial dipole oscillation frequency can be seen in the oscillations of the field envelope near $t = \tau = 0$. At large t and $|\tau|$, the signal field envelope is not amplitude modulated at electronic frequencies, but the signal fields are still phase modulated.

dynamics (using only the refractive index and frequency) to reveal the nonlinear polarization.

The role of the transition dipole product in altering the phase of a four-wave-mixing signal is interesting because it may provide a way to measure the relative phase of four different transition dipole matrix elements. For example, it may be possible to measure the relative signs of four different Franck-Condon overlap integrals in an electronic transition by phase-resolved four-wave mixing (the product also appears in quantum beats). This vibronic transition dipole product is included semiclassically in the numerical calcula-

tions presented here, and may underlie the negative pump-probe signals previously calculated for a two-electronic-state system at low temperature [61]. The negative signals in these nonperturbative calculations of pump-probe signals were interpreted as resulting from absorption increases caused by population transfer to unpopulated vibrational levels though impulsive stimulated Raman scattering.

The utility of the delay dependent phase modulation becomes apparent when δ-function pulses are considered. Then the third-order polarization $P^{(3)} = (S^{(3)} + \text{c.c.})$ exhibits a pulse-delay-dependent phase shift $\omega_{eg}\tau$ at the Bohr fre-

quency of the initially excited dipole even while emitting at a different frequency. In the fully noncollinear case, these optical frequency oscillations which encode the initial excitation frequency occur only in the phase of the polarization and not in the amplitude. Since the pioneering work of Ref. [1], most treatments of photon echoes have followed Hahn's treatment of spin echoes in the rotating frame [92]. Many equations for nonlinear optical signals assume delays of the carrier wave type generated in magnetic resonance [38]. Some expressions for the third-order polarization or emitted field explicitly differ from Eq. (8) only by predicting a phase modulation at $(\omega_{eg} - \omega_0)\tau$, where ω_0 is the carrier frequency of the excitation pulses [e.g., Ref. [49], Eq. (21.22); Ref. [41] (Eq. 10.13)]. These equations predict the signal phase when carrier wave pulse delays are used (e.g., nuclear magnetic resonance, the optical experiments of Warren and Zewail [46]). The cosinusoidal phase modulation at $(\omega_{eg} - \omega_0)\tau$ for carrier wave delays does not reveal the sign of $(\omega_{eg} - \omega_0)$. [93] In contrast, Eq. (8) shows that phase modulation as a function of τ generated by envelope delayed pulses provides absolute frequencies ω_{eg}.

Although their equation for the polarization was written in the rotating frame, the authors of Ref. [12] clearly discussed phase modulation of the polarization as a function of τ in the lab frame for two pulse echos. For an inhomogeneously broadened sample, signal phase modulation at the initial electronic frequency *produces* photon echos. The situation for three-pulse echoes is somewhat different because they can persist after electronic coherence is gone [4]. In particular, echo amplitude beats have been observed as a function of τ for T exceeding the upper state lifetime T_1 [8,9], and the initial electronic frequency has been recovered from a phase-modulated signal for which T exceeded the electronic dephasing time T_2 [36]. The storage of the electronic frequency-dependent phase can be illuminated by considering interference between single spectral components of crossing plane waves [36]. Crossing waves produce a spatial intensity grating $I(\mathbf{r}) = 2I(1 + \cos[(\mathbf{k}_a - \mathbf{k}_b) \cdot \mathbf{r} - \omega\tau])$, where I is the intensity of a single beam, ω is the frequency, and τ is the delay produced by path-length differences at $\mathbf{r} = \mathbf{0}$. As τ increases, the grating maxima move continuously along the direction $\mathbf{k}_a - \mathbf{k}_b$, so that $\omega\tau$ can be regarded as the phase of the grating. For excitation of an inhomogeneously broadened two-level system by broadband pulses, each resonant frequency produces an independent population grating with phase $\omega_{eg}\tau$. A grating phase shift ϕ leads to a phase shift $m\phi$ in the mth order of diffraction. Phase modulation of the population grating, which is stored in the spatial position of the excited and unexcited molecules, translates directly into phase modulation of the scattered signal field [38]. It should be emphasized that phase modulation at the initial dipole oscillation frequency can be observed with a third pulse even after *all* molecular coherences have been destroyed.

When the first two excitation pulses are collinear, the superposition of noncollinear phase-modulated signals produces an amplitude and phase modulated signal. Comparing Eqs. (5) and (6), a signal generated by collinear pulses a and b may exist for all six pulse orderings. The four orderings with $\tau_c > \tau_a$ or $\tau_c > \tau_b$ [the bottom four terms in Eqs. (5) and

(6)] contain phase-modulated contributions from only one of the two noncollinear signals, and will remain phase modulated in the collinear case. In contrast, the two orderings with $\tau_a > \tau_c$ and $\tau_b > \tau_c$ [the two top terms in Eqs. (5) and (6)] will have oppositely phase-modulated contributions from *both* noncollinear signals. The sum of these two oppositely phase-modulated signals will be at least partially amplitude modulated, so the collinear signal will be both amplitude and phase modulated. Another valid view is that the collinear amplitude modulation simply results from the excitation source (pulses a and b) blinking on and off throughout the sample as the delay is varied. The description of amplitude modulation as arising from superposition of two oppositely phase-modulated signals is valuable because it emphasizes the role of the material. As an example, a material with a resonance which is narrow compared to the pulse spectrum can produce amplitude-modulated signals which persist outside the range of temporal pulse overlap. This result can be understood from a frequency domain view: the spectral components which excite the material will all blink together until the interpulse delay exceeds the inverse linewidth of the transition. Frequency- and delay-dependent modulation of the position of excited molecules within the sample in the noncollinear case becomes modulation of the excited state population throughout the sample for collinear excitation.

In the absence of relaxation, the final frequency can involve both new upper and new lower states ($\omega_{e'g'}$) for $\tau > 0$. $V(\omega_{e'g})$ or $\Lambda(\omega_{eg'})$ double resonances with one common level can appear for all τ. The four-level parallel four-wave-mixing signal (ω_{eg} and $\omega_{e'g'}$) in the absence of relaxation has no frequency domain double resonance analog but is known from investigations of CARS/CSRS [67,70,71] and multilevel interference effects in photon echoes (see references in Mitsunaga, Kintzer, and Brewer [45]), and provides valuable information about the level structure. When cross-relaxation takes place during T, the signal can involve new upper and lower states for any τ. The signal phase modulation with τ provides a way to connect the final emission frequency to the frequency of the initial dipole oscillation which caused it. This correlation of initial and final frequencies under the inhomogeneous linewidth provides not only the difference frequencies seen in intensity beats [8,12,14], but also absolute frequency information not present in difference frequency beats. This correlation is conveniently represented in the frequency domain by two-dimensional Fourier transformation [36,55,70,94]. Femtosecond 2D Fourier transform spectroscopy should be a useful probe of correlation, disorder, and electronic coupling, and their time development [10,15–17].

A few macroscopic factors which influence the phase of the signal have not been treated here. Perhaps the most obvious are phase mismatch and propagation/depletion of the waves as they travel through the sample. The finite beam diameter can also give rise to phase shifts (e.g., Guoy phase shift in passing through a focus) [65]. The combined effect of spatial and polarization radiation phase shifts merits investigation using the slowly evolving wave approximation developed by Brabec and Krausz [54,81,82]. The influence

of crossing angle broadening and dependence of the signal diffraction angle on frequency also deserve exploration.

V. CONCLUSION

Five sources of constant phase shifts for resonant, fully phase-matched, noncollinear four-wave-mixing signals have been identified: the signs of the frequencies (absorption vs emission); the phases of the excitation pulses; the transition dipole product; coherence oscillation during the delays between pulses; and the spontaneous radiation dynamics of the nonlinear polarization. These factors are all relevant to experiments with a broadband phase-matching geometry on optically thin samples: phase matching and propagation issues add further complexity. The excitation pulse phase can, in principle, be experimentally controlled, and may be useful for separating different types of signals. The effects of spontaneous radiation dynamics can be removed in the frequency domain. The electric fields of noncollinear four-wave-mixing signals are phase modulated at the initial dipole oscillation frequency by the delay τ between the first two pulses.

There is a simple physical picture of this phase modulation. The first pulse excites coherently oscillating dipoles throughout the sample. The second pulse stores the dipole phase in the frequency-dependent, periodically modulated position of excited molecules within the sample. Upon excitation by a third pulse, this molecular excitation grating acts as a source of spontaneous radiation which imprints the grating phase onto the phase of the diffracted signal. It is important to emphasize that the initial dipole phase can be recovered by the third pulse even after *all* molecular coherence has been destroyed. If the signal field (including constant phase shifts relative to the excitation pulses) is measured for a series of delays, the signal can be separated according to the coherence oscillation frequency by Fourier transformation with respect to the pulse delay. This provides a route to frequency resolution within the pulse spectrum in nonlinear spectroscopy. Similar labeling is possible using a closely related amplitude modulation of signals in partially collinear geometries. Coherence labeling should be valuable for studies of level structure, vibrational and excitonic coupling, relaxation dynamics, and examination of correlations hidden by inhomogeneous broadening.

ACKNOWLEDGMENTS

APPENDIX: BROWNIAN OSCILLATOR MODEL

The calculations presented here used the Brownian oscillator model, which predicts the optical properties of a two-level system that is linearly coupled to coordinates which interact with a heat bath of harmonic oscillators. This is a reasonable model for the electronic states of molecules in condensed phases. A fundamental quantity in the Brownian oscillator model for four-wave-mixing signals is the Bohr transition frequency correlation function $M(t)$,

$$M(t) = \frac{\langle \Delta\omega(0)\Delta\omega(t)\rangle}{\langle \Delta\omega^2 \rangle}, \tag{A1}$$

where $\Delta\omega(t) = \langle\omega\rangle - \omega(t)$ [60]. $\langle\omega\rangle$ is the average transition frequency, and the brackets indicate an average over the ground-electronic-state coordinate probability density. Since $M(t)$ is a correlation function, $M(0) = 1$ and $[dM/dt]_{t=0} = 0$. Physically, the electronic excitation of the chromophore is too fast for the nuclei to respond instantaneously.

The multimode Brownian oscillator model uses a frequency correlation function $M_i(t)$ for each mode i. The correlation functions for damped harmonic motion are given in Eq. (20) of Ref. [95]. In the high temperature ($k_B T/\hbar > \omega_i$) limit, the homogeneous line-shape function for each mode, $g_i(t)$, is given by [95]
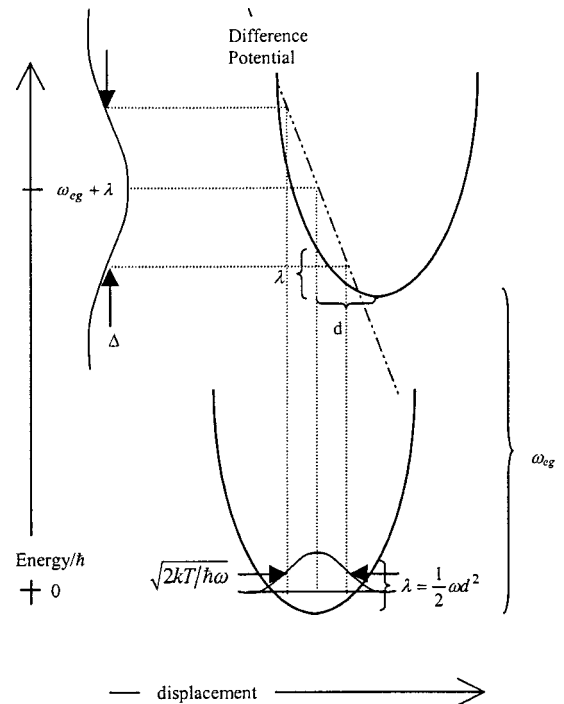
FIG. 7. Illustration of Brownian oscillator parameters and semiclassical Franck-Condon mapping between coordinates and frequency. The upper and lower electronic potential curves have the same harmonic vibrational frequency ω_v, different equilibrium positions separated by a displacement d, and an energy gap of $\hbar\omega_{eg}$ between minima. The difference potential $V_e(q) - V_g(q)$ is represented by the dot-dashed line. The solid curve on the lower potential represents the classical thermal distribution of vibrational coordinates at temperature T. The width of the absorption spectrum on the left is dictated by a Franck-Condon mapping (shown by dotted lines) of coordinates to frequencies using the difference potential. Δ determines the width of the absorption spectrum, which is centered at frequency $(\omega_{eg} + \lambda)$.

$$g_i(t) = i\lambda_i \int_0^t dt_1 M_i(t_1) + \Delta_i^2 \int_0^t \int_0^{t_1} dt_1 dt_2 M_i(t_2).$$
$$(A2)$$

λ_i is the reorganization energy of mode i, and Δ_i^2 is the coupling strength of the ith mode to the bath. The Brownian oscillator line-shape functions used in these calculations assume the bath has no memory of earlier states of the system, and are valid only in the high-temperature limit [96,97].

Figure 7 illustrates the Brownian oscillator parameters. It is assumed that the ground- and excited-state potentials are harmonic with the same vibrational frequencies ω_i. Each oscillator is displaced by the dimensionless normal mode displacement d_i, so that $\lambda_i = (1/2)\omega_i d_i^2$, and the total Stokes shift is $2\lambda = 2\Sigma\lambda_i$. In the semiclassical (high temperature) limit, λ and Δ^2 are related by $\Delta_i^2 = 2(k_B T/\hbar)\lambda_i$ [95]. The width of the spectrum can also be obtained by classical Franck-Condon coordinate-frequency mapping $\omega(q) = [V_e(q) - V_g(q)]/\hbar$ [98]. The classical thermal distribution of vibrational displacements q is given by $P(q) = \sqrt{\hbar\omega_v/2\pi kT} \exp[-\hbar\omega_v q^2/2kT]$. The absorption lineshape $g(\omega)$ can be expressed as $g(\omega) \propto -P(q)/(d\omega/dq) = P(q(\omega))/\omega_i d$, where $q(\omega) = (\omega_{eg} + \lambda - \omega)/\omega_i d$ is

an inverse function of $\omega(q) = (\omega_{eg} + \lambda - \omega_i q d_i)$. This yields $g(\omega) \propto \exp[-(\omega - (\omega_{eg} + \lambda))^2/2\Delta^2]$, where $\Delta^2 = 2(k_B T/\hbar)\lambda$.

The overall homogeneous line-shape function in the multimode Brownian oscillator model is given by $g(t) = \Sigma g_i(t)$. The steady-state absorption and emission lineshapes (for Einstein B) are

$$g_a(\omega) \propto \frac{1}{\pi} \text{Re}\left\{ \int_0^\infty dt \exp[-i(\omega - \omega_{eg})t]\exp[-g(t)] \right\},$$

$$g_f(\omega) \propto \frac{1}{\pi} \text{Re}\left\{ \int_0^\infty dt \exp[-i(\omega - \omega_{eg})t]\exp[-g*(t)] \right\}.$$
$$(A3)$$

Since the additive line-shape function $g(t)$ appears in an exponential that is Fourier transformed to yield the spectrum, the effect of each mode on the spectrum is a convolution. The imaginary part of $g(t)$ determines the center frequency of a transition, while the real part determines the width. Expressions for the third-order impulse response functions R_i in Eq. (3) in terms of the line-shape function $g(t)$ may be found in Eq. (8.15) of Mukamel's monograph [41].

[1] I. D. Abella, N. A. Kurnit, and S. R. Hartmann, Phys. Rev. **141**, 391 (1966).

[2] P. R. Berman, J. M. Levy, and R. G. Brewer, Phys. Rev. A **11**, 1668 (1975).

[3] T. Yajima and Y. Taira, J. Phys. Soc. Jpn. **47**, 1620 (1979).

[4] T. W. Mossberg, R. Kachru, S. R. Hartmann, and A. M. Flusberg, Phys. Rev. A **20**, 1976 (1979).

[5] A. M. Weiner, S. Desilvestri, and E. P. Ippen, J. Opt. Soc. Am. B **2**, 654 (1985).

[6] P. C. Becker, H. L. Fragnito, J. Y. Bigot, C. H. B. Cruz, R. L. Fork, and C. V. Shank, Phys. Rev. Lett. **63**, 505 (1989).

[7] J.-Y. Bigot, M. T. Portella, R. W. Schoenlein, C. J. Bardeen, A. Migus, and C. V. Shank, Phys. Rev. Lett. **66**, 1138 (1991).

[8] M. K. Kim and R. Kachru, Phys. Rev. B **44**, 9826 (1991).

[9] M. Mitsunaga, R. Yano, and N. Uesugi, Phys. Rev. B **45**, 12 760 (1992).

[10] M. Koch, J. Feldmann, G. von Plessen, E. O. Göbel, and P. Thomas, Phys. Rev. Lett. **69**, 3631 (1992).

[11] L. Q. Lambert, A. Compaan, and I. D. Abella, Phys. Rev. A **4**, 2022 (1971).

[12] A. Schenzle, S. Grossman, and R. G. Brewer, Phys. Rev. A **13**, 1891 (1976).

[13] R. L. Shoemaker, Annu. Rev. Phys. Chem. **30**, 239 (1979).

[14] Y. C. Chen, K. Chiang, and S. R. Hartmann, Phys. Rev. B **21**, 40 (1980).

[15] J. Erland and I. Balshev, Phys. Rev. A **48**, R1765 (1993).

[16] X. Zhu, M. S. Hybertsen, and P. B. Littlewood, Phys. Rev. Lett. **73**, 209 (1994).

[17] M. Koch, J. Feldmann, G. von Plessen, S. T. Cundiff, E. O. Göbel, P. Thomas, and K. Köhler, Phys. Rev. Lett. **73**, 210 (1994).

[18] L. Xu, C. Spielmann, A. Poppe, T. Brabec, F. Krausz, and T. W. Hänsch, Opt. Lett. **21**, 2008 (1996).

[19] D. J. Kane and R. Trebino, IEEE J. Quantum Electron. **29**, 571 (1993).

[20] J. Paye, IEEE J. Quantum Electron. **30**, 2693 (1994).

[21] L. Lepetit, G. Chériaux, and M. Joffre, J. Opt. Soc. Am. B **12**, 2467 (1995).

[22] G. Taft *et al.*, IEEE J. Sel. Top. Quantum Electron. **2**, 575 (1996).

[23] R. Trebino, K. W. DeLong, D. N. Fittinghoff, J. N. Sweetser, M. A. Krumbügel, B. A. Richman, and D. J. Kane, Rev. Sci. Instrum. **68**, 3277 (1997).

[24] C. Iaconis and I. A. Walmsley, Opt. Lett. **23**, 792 (1998).

[25] Z. Cheng, A. Fürbach, S. Sartania, M. Lenzer, C. Spielmann, and F. Krausz, Opt. Lett. **24**, 247 (1999).

[26] A. Baltuska, M. S. Pshenichnikov, and D. A. Wiersma, IEEE J. Quantum Electron. **35**, 459 (1999).

[27] E. Tokunaga, A. Terasaki, and T. Kobayashi, Opt. Lett. **17**, 1131 (1992).

[28] D. S. Chemla, J.-Y. Bigot, M.-A. Mycek, S. Weiss, and W. Schäfer, Phys. Rev. B **50**, 8439 (1994).

[29] E. Tokunaga, A. Terasaki, V. S. Valencia, T. Wada, H. Sasabe, and T. Kobayashi, Appl. Phys. B: Lasers Opt. **63**, 255 (1996).

[30] L. Lepetit, G. Chériaux, and M. Joffre, J. Nonlinear Opt. Phys. Mater. **5**, 465 (1996).

[31] J.-P. Likforman, M. Joffre, and V. Thierry-Mieg, Opt. Lett. **22**, 1104 (1997).

[32] M. F. Emde, W. P. de Boeij, M. S. Pshenichnikov, and D. A. Wiersma, Opt. Lett. **22**, 1338 (1997).

[33] X. Chen, W. J. Walecki, O. Buccafusca, D. N. Fittinghoff, and A. L. Smirl, Phys. Rev. B **56**, 9738 (1997).

[34] A. L. Smirl, X. Chen, and O. Buccafusca, Opt. Lett. **23**, 1120 (1998).

[35] S. M. Gallagher, A. W. Albrecht, J. D. Hybl, B. L. Landin, B. Rajaram, and D. M. Jonas, J. Opt. Soc. Am. B **15**, 2338 (1998).

[36] J. D. Hybl, A. W. Albrecht, S. M. Gallagher Faeder, and D. M. Jonas, Chem. Phys. Lett. **297**, 307 (1998).

[37] S. Mukamel, C. Ciordas-Ciurdariu, and V. Khidekel, IEEE J. Quantum Electron. **32**, 1278 (1996).

[38] A. Albrecht, J. D. Hybl, S. M. Gallagher Faeder, and D. M. Jonas, J. Chem. Phys. **111**, 10 934 (1999).

[39] J. A. Armstrong, N. Bloembergen, J. Ducuing, and P. S. Pershan, Phys. Rev. **127**, 1918 (1962).

[40] D. Lee and A. C. Albrecht, Adv. Chem. Phys. **83**, 43 (1993). Some results in this paper differ superficially from those given here, because Lee and Albrecht defined the phase of the nonlinear polarization as the signed sum of the excitation pulse phases, and incorporated the phase of the susceptibility into the phase shift between the polarization and emitted field.

[41] S. Mukamel, *Principles of Nonlinear Optical Spectroscopy* (Oxford University Press, New York, 1995).

[42] M. Cho, N. F. Scherer, G. R. Fleming, and S. Mukamel, J. Chem. Phys. **96**, 5618 (1992).

[43] W. P. de Boeij, M. A. Pshenichnikov, and D. A. Wiersma, Chem. Phys. **233**, 287 (1998).

[44] K. A. Nelson, R. Casalegno, R. J. D. Miller, and M. D. Fayer, J. Chem. Phys. **77**, 1144 (1982).

[45] M. Mitsunaga, E. S. Kintzer, and R. G. Brewer, Phys. Rev. B **31**, 6947 (1985).

[46] W. S. Warren and A. H. Zewail, J. Chem. Phys. **78**, 2279 (1983).

[47] A. M. Weiner, IEEE J. Quantum Electron. **QE-19**, 1276 (1983).

[48] J. A. McGuire, W. Beck, X. Wei, and Y. R. Shen, Opt. Lett. **24**, 1877 (1999). This experiment was based on signal intensity modulation with delay between a collinear pulse pair where the wave vector of the *pulse pair* appears only once in the signal wave vector. In all the other experiments discussed here, the wave vector of *each pulse* appears separately in the signal wave vector.

[49] Y. R. Shen, *The Principles of Nonlinear Optics* (Wiley-Interscience, New York, 1984).

[50] P. Vöhringer, D. C. Arnett, T.-S. Yang, and N. F. Scherer, Chem. Phys. Lett. **237**, 387 (1995).

[51] W. P. de Boeij, M. S. Pshenichnikov, and D. A. Wiersma, J. Phys. Chem. **100**, 11 806 (1996).

[52] H. Petek and S. Ogawa, Prog. Surf. Sci. **56**, 239 (1997).

[53] B. Bousquet, L. Canioni, and L. Sarger, J. Chem. Phys. **109**, 7319 (1998).

[54] T. Brabec and F. Krausz, Phys. Rev. Lett. **78**, 3282 (1997).

[55] S. M. Gallagher Faeder and D. M. Jonas, J. Phys. Chem. A **103**, 10 489 (1999).

[56] V. Volterra, *Theory of Functionals* (Blackie and Son, London, 1930).

[57] P. N. Butcher and D. Cotter, *The Elements of Nonlinear Optics* (Cambridge University Press, New York, 1991).

[58] For resonant linear absorption of a Gaussian pulse with a field-envelope full width at half maximum equal to one optical cycle, the rotating-wave approximation gives the excited-state coefficient to better than one part in 10^6 in the limit of vanishing damping.

[59] A. Yariv, *Quantum Electronics* (Wiley, New York, 1975).

[60] T. Joo, Y. Jia, J.-Y. Yu, M. J. Lang, and G. R. Fleming, J. Chem. Phys. **104**, 6089 (1996). We thank Professor Taiha Joo for verifying parameters $\Delta = 245$ cm^{-1} in Fig. 8, detuning $\delta\omega = 132.5$ cm^{-1} in Fig. 9(b), and confirming errors in Fig. 10 (which should show $R_1 = R_4$ and $R_2 = R_3$ at $T = 0$) and Fig. 11.

[61] D. M. Jonas, S. E. Bradforth, S. A. Passino, and G. R. Fleming, J. Phys. Chem. **99**, 2594 (1995).

[62] J. G. Fujimoto and T. K. S. Lee, IEEE J. Quantum Electron. **QE-22**, 1215 (1986).

[63] W. P. de Boeij, M. S. Pshenichnikov, K. Duppen, and D. A. Wiersma, Chem. Phys. Lett. **224**, 243 (1994).

[64] W. de Boeij, M. S. Pshenichnikov, and D. A. Wiersma, Chem. Phys. Lett. **247**, 264 (1995).

[65] A. E. Siegman, *Lasers* (University Science Books, Mill Valley, CA, 1986).

[66] R. P. Feynman, R. B. Leighton, and M. Sands, *The Feynman Lectures on Physics* (Addison-Wesley, Reading, MA, 1977).

[67] D. S. Alavi, R. S. Hartman, and D. H. Waldeck, J. Chem. Phys. **92**, 4055 (1990).

[68] R. S. Francis, G. Hinze, and M. D. Fayer, Chem. Phys. Lett. **304**, 28 (1999).

[69] D. P. Weitekamp, Adv. Magn. Reson. **11**, 111 (1983).

[70] R. R. Ernst, G. Bodenhausen, and A. Wokaun, *Principles of Nuclear Magnetic Resonance in One and Two Dimensions* (Oxford University Press, London, 1987).

[71] H. Kawashima, M. M. Wefers, and K. A. Nelson, Annu. Rev. Phys. Chem. **46**, 627 (1995).

[72] W. Demtröder, *Laser Spectroscopy* (Springer-Verlag, New York, 1982).

[73] G. Bodenhausen, R. Freeman, G. A. Morris, and D. L. Turner, J. Magn. Reson. **31**, 75 (1978).

[74] J. K. Steehler and J. C. Wright, J. Chem. Phys. **83**, 3200 (1985).

[75] M. T. Riebe and J. C. Wright, J. Chem. Phys. **88**, 2981 (1988).

[76] A. M. Bacon, H. Z. Zhao, P. J. Laverty, L. J. Wang, and J. E. Thomas, Phys. Rev. A **49**, 379 (1994).

[77] E. Gershgoren, E. Gordon, and S. Ruhman, J. Chem. Phys. **106**, 4806 (1997).

[78] T. Tokizaki, T. Makimura, H. Akiyama, A. Nakamura, K. Tanimura, and N. Itoh, Phys. Rev. Lett. **67**, 2701 (1991).

[79] D. M. Jonas, M. J. Lang, Y. Nagasawa, T. Joo, and G. R. Fleming, J. Phys. Chem. **100**, 12 660 (1996).

[80] J. M. Blatt and V. F. Weisskopf, *Theoretical Nuclear Physics* (Dover, New York, 1991).

[81] M. A. Porras, J. Opt. Soc. Am. B **16**, 1468 (1999).

[82] Q. Lin and E. Wintner, Opt. Commun. **150**, 185 (1998).

[83] H. J. Bakker, P. C. M. Planken, L. Kuipers, and A. Langendijk, Phys. Rev. A **42**, 4085 (1990).

[84] The integration over δ functions placed at discontinuities in the nonlinear response function is subtle because the standard result $\int \delta(x)f(x)dx = f(0)$ requires that f be continuous near 0. For the Heaviside step function $\theta(x)$, the definition of the δ-function integral via a limiting series of integrals with narrow symmetric test functions $\delta_n(x)$ yields $\int \delta(x)\theta(x)dx = \frac{1}{2}$. When improperly time-ordered diagrams are included, this evaluation of the δ-function integrals at discontinuities naturally leads to analytic results that agree with numerical integration over sufficiently short symmetric pulses. At $T = 0$,

these δ-function results differ from those given previously by us [36] and others. [41,60] For consistency, a limiting series of integrals could also be used to define the response function in terms of the polarization at discontinuities.

[85] W. H. Press, S. A. Teukolsky, W. T. Vetterling, and B. P. Flannery, *Numerical Recipes* (Cambridge University Press, Cambridge, 1987).

[86] P. Cong, Y. J. Yan, H. P. Deuel, and J. D. Simon, J. Chem. Phys. **100**, 7855 (1994).

[87] S. M. Gallagher Faeder, Ph.D. thesis, University of Colorado, Boulder, CO, 1999.

[88] D. A. Wiersma and K. Duppen, Science **237**, 1147 (1987).

[89] J. D. Hybl, S. M. G. Faeder, A. W. Albrecht, C. A. Tolbert, D. C. Green, and D. M. Jonas, J. Lumin. **87-89**, 126 (2000).

[90] In contrast, for δ-function pulses at $T=0$, the amplitude modulation is incomplete for nonzero τ because the twofold jumps in the phase-modulated signals occur on opposite sides of $\tau = 0$. This result seems peculiar because the entire resonant part of the pulse pair frequency spectrum can blink on and off long after the pulses have ceased to overlap. However, there is a 50:50 chance that the dipole interference of the second pulse in the pump pair will be ''blocked'' by a simultaneous probe. The amplitude modulated three pulse experiments in Refs. [32], [43], [64] do not include results with $T<t_p$, but this prediction could be experimentally tested with transform-limited broadband excitation of a narrow resonance.

[91] G. Hinze, R. S. Francis, and M. D. Fayer, J. Chem. Phys. **111**, 2710 (1999).

[92] E. L. Hahn, Phys. Rev. **80**, 580 (1950).

[93] An additional experiment with pulse a or b phase shifted by $\pi/2$ can generate sinusoidal phase modulation at $(\omega_{eg}-\omega_0)\tau$ to independently determine the signs of $(\omega_{eg}-\omega_0)$ and the transition dipole product. This is known as phase cycling in NMR [70].

[94] W. M. Zhang, V. Chernyak, and S. Mukamel, J. Chem. Phys. **110**, 5011 (1999).

[95] S. Mukamel, Annu. Rev. Phys. Chem. **41**, 647 (1990).

[96] Y. Tanimura and S. Mukamel, Phys. Rev. E **47**, 118 (1993).

[97] Y. Gu, A. Widom, and P. M. Champion, J. Chem. Phys. **100**, 2547 (1994).

[98] J. Tellinghuisen, J. Mol. Spectrosc. **103**, 455 (1984).